MODELING THE INTERFACE BETWEEN SHELL AND SOLID ELEMENTS

Mr. Denis J. Feld, Engineer Principal
Mr. Jean G. Soudry, Section Head - Structures

Goodyear Aerospace Corporation
Akron, Ohio

In many practical finite element models, some portions of the structure are best modeled with shell elements and others with solids. This paper evaluates several alternatives to modeling the interface between the shell and solid elements. The alternative methods are screened on a simple Timoshenko beam whose solution is known. It is demonstrated that there are acceptable and poor methods of modeling the interface. The acceptable methods are characterized by satisfying kinematic relationships of displacements between the solid and shell elements - without overconstraint. A plate finite element model loaded in bending is used to further verify the acceptability of using the NASTRAN rigid elements at the interface of shell and solid elements. Two basic methods applicable to a wide range of modeling situations are suggested. Either RBAR or RBE3 interfaces produce acceptable results if properly applied.

1. INTRODUCTION

The finite element analyst is frequently faced with structures that have some segments, best modeled with shell elements, while others are best modeled with solids. For example, the finite element model in Figure 1 has segments that are relatively thin, where the assumption of a two-dimensional stress state or shell elements is preferred. Other segments are relatively thick and have a complex three-dimensional state of stress. These segments are modeled with solid elements. This paper addresses modeling methods for the interface between the plate and shell elements, using the rigid elements of MSC/NASTRAN.

The interface must allow for the transfer of in-plane moments in shell elements with rotational degrees of freedom. Solid elements, which have no rotational freedoms, can accept the moments from neighboring plates by introducing force couples. It is the function of the NASTRAN rigid elements to introduce moments from shell elements as force couples to the solid elements. A workable interface of rigid elements must also not create significant perturbations to the stresses in the shell and solid elements.

Many alternatives, using the NASTRAN rigid elements or multipoint constraint equations, are possible. Some alternatives and examples of both good and poor approaches are presented. Suggested approaches are chosen on the basis of continuity of stress between solid and shell elements, insignificant perturbation of stresses, and simplicity in applying to real modeling situations. A simple cantilever beam model is used to screen candidate interface approaches. The better approaches are then verified or modified on a rectangular plate with simply supported edges.

2. CANTILEVER BEAM SCREENING MODEL

An eight-inch-long aluminum cantilever beam is used to screen candidate interfaces of rigid elements. A rectangular 1 by 0.25-inch cross section is used. Young's modulus is 10^7 psi, and Poisson's ratio is 0.3. The beam is loaded by 60 pounds at the tip in the axial direction and in the two bending planes as three separate subcases.

2.1 Theoretical Solution - Simple beam theory provides the deflection, axial stress, and bending stresses given in Figure 2. Bending deflections ignore transverse shear. It is important to note the assumptions of simple bending stress: Plane sections remain plane after bending, and end effects are not considered.

2.2 Finite Element Models - Since results of the finite element solutions are compared to those of a simpler theory, which includes no beam end effects, care must be taken in providing the cantilever constraint. Consider the stress distribution under simple bending, as shown in Figure 3. Because of the Poisson effect, the beam cross section undergoes the deformation depicted. All the beam finite element models in this study remove end effects at the cantilever end by allowing cross-section deformation. This is accomplished by applying three multipoint constraint equations to force the average y and z displacement and rotation about the x axis of grid points at the cantilever end to zero. The rotational constraint equation is expressed as $\sum_{i=1}^{n} \bar{\delta}_i \times \bar{r}_i = 0$, where n is the number of grid points in the cantilever end, $\bar{\delta}_i$ is the vector sum of the x and y-displacements, and $\bar{r}_i$ is the vector to grid point i. In addition, x-translation degrees of freedom at the cantilever end are constrained by SPC.

The finite element models are shown in Figure 4A through 4E. The H20 and H8 models contain no shell elements and simply provide a qualitative baseline against which to evaluate the models using interfaces. They are the H20Q4 model interfacing 20-node HEXA and QUAD4 elements; the H20Q8 model with 20-node HEXA and QUAD8; and the H8Q4 model with 8-node HEXA and QUAD4 elements. The element coordinate system used for reporting stresses is the same as the basic system shown in Figure 2. Normal and shear stress for solid and shell elements follows the NASTRAN conventions. Transverse shear flexibility for the shells is not included.

More emphasis is given in this study to the H20Q4 model. It will be seen that interfaces for the H20Q8 and H8Q4 models are relatively straightforward. The alternative approaches to modeling the interface are identified by case numbers in this study. Results shown for the alternative cases do not include stress values that are small and insignificant.

2.2.1 Baseline H20 Model - The baseline H20 finite element model of Figure 4A is used to compare results of interfaces for the H20Q4 and H20Q8 models. The axial and bending loads are distributed over the beam tip element face with PLOAD4 bulk data cards for each of the three subcases. The results for each subcase are shown in Figure 5. σ_{xx} is seen to follow theoretical values closely for all subcases for the whole beam length. The other normal stresses are small in comparison to σ_{xx}, as expected. Shear stresses are small and are not plotted.

2.2.2 QUAD4 to 20-Node HEXA Interface - The H20Q4 model is shown in Figure 4B. Loads are applied equally to the two grid points at the beam tip. This model is used for Cases 1 through 6.

Case 1 - The interface area for Case 1 is illustrated in Figure 6. RBAR rigid elements connect grid points at the beam center to the upper and lower grid points on the solid elements. Note that the RBAR's do not constrain displacement in the thickness direction of the solids in order to accommodate the Poisson effect. Physically, this may be thought of as a telescoping rigid bar, as indicated. Also note that the shell corners and solid center edges at the interface share common grid point identities (GP 7 and

8). The RBAR's ensure that grid points 7, 9, 11 and 8, 10, 12 on the HEXA element remain in a straight line after deformation. This is consistent with the assumption used in shell elements that normals to the plane of the shell remain normal after deformation. The upper and lower edge grid points on the solids, 21 and 24, at the interface are unconstrained for this case. Results of the finite element model are shown in Figure 7. Undesirable stress behavior near the interface in the HEXA elements is noted for this case. This behavior can be traced to the deflection behavior on the solid element at the interface shown in the inset. The middle edge grid points, 21 and 24, do not follow a linear pattern across the width of the beam and are thus not compatible with the displacement field of the QUAD4 shell element. The problem here is analogous to changing the order of neighboring elements. An alternative to force compatibility across the width of the interface is introduced in Case 2.

Case 2 - The RBAR's in the shell/solid interface for Case 2 are identical to those of Case 1. The upper and lower grid points, 21 and 24, on the HEXA element are deleted to force compatibility across the beam width between the QUAD4 and HEXA elements, shown in Figure 8. Acceptable results with this interface are shown for the beam in Figure 9. However, it will be seen that undesirable stresses are introduced when interface for this case is used under the more complex plate load conditions. Alternatives to complete deletion of the upper and lower edge grid points are examined in Section 3.2.2.

Case 3 - In Case 3, a deliberate overconstraint is introduced at the interface through the RBAR elements. The H20Q4 model is used, and the "telescoping" character of the RBAR's is removed so that changes in beam thickness from the Poisson effect are not permitted. Otherwise, the interface shown in Figure 10 is the same as Case 2, which produced acceptable results. The increased stresses introduced through the overconstraint are shown in Figure 11.

Case 4 - An example of severe overconstraint in the interface is shown in Figure 12. Here, the entire interface is a rigid RBE2 element. Not only is the thickness not permitted to change in response to the Poisson effect, but the cross-section also is not permitted to deform as indicated in Figure 3. As expected, severe perturbation to the results is seen in Figure 13.

Case 5 - While the interface of Case 2 produced acceptable results, it is desired to examine an alternative to improve accuracy. The RBAR's for Case 5 are identical to those in Case 2, as are deleted nodes 21 and 24 at the upper and lower edge of the HEXA element. However, separate grid point identities are maintained at the interface for the solid and shell elements. This is shown in Figure 14. Multipoint constraint equations are used to force grid points 7 and 8 z-displacements to be the average of grid points 9, 11, 22 and 10, 12, and 23, respectively. This allows force in the z direction from the shell to be distributed through the thickness of the solid, as opposed to being concentrated at the grid points 7 and 9 in Case 2. Additional zero length RBAR's are needed to tie together the x and y displacements of grid points 7 to 22 and 8 to 23. No significant improvement in accuracy of the stress results is noted in comparing Figure 15 to the Case 2 results of Figure 9. Thus, this complication is not worthwhile.

Case 6 - A different type of constraint is illustrated in Figure 16. An RBE3 element, wherein displacements and rotations on the shell interface grid points are determined from a least square weighted average of displacements of the solid element grid points, is used. The upper and lower HEXA interface grid points, 21 and 24, are deleted to

force compatibility between the QUAD4 and HEXA elements. Grid points at the mid-plane of the beam at the interface have separate identities (for example, 7, 22 and 8, 23). To prevent instability of the RBE3 elements in rotation about its own axis, the shell normal degree of freedom, 6, is included in the C1, not the REFC set on the RBE3 bulk data cards. An equal weighting factor is used for all grid points on the HEXA elements. Unlike Case 2, all points on the RBE3 elements need not be on a straight line after deformation. This is tantamount to relaxation of the constraint which is present in previous cases - that normals to the shell remain normal after deformation. Perturbation to the stresses under normal bending loads near the interface is not significant, as seen in Figure 17.

Under axial load, the σ_{zx} shear stresses are larger than those found in Case 2 RBAR configuration. This results from the RBE3 grid points not remaining on a straight line after deformation. In applications where shell elements carry significant in-plane stresses, the reader should consider the σ_{zx} perturbation in deciding between RBAR and RBE3 interfaces.

2.2.3 Baseline H8 Model - Results from the H8 model, composed entirely of 8-node HEXA elements illustrated in Figure 4C, are used for qualitative evaluation of interfaces on H8Q4 models. Loads at the beam tip are distributed by using PLOAD4 cards. Results are given in Figure 18.

2.2.4 QUAD4 to 8-Node HEXA Interface - When QUAD4 and 8-node HEXA elements are interfaced, there are no complications caused by the upper and lower edge nodes, as in the previous cases. The H8Q4 model illustrated in Figure 4D is used for the shell/solid interfaces in Cases 7, 8, and 9.

Case 7 - RBAR's are used to connect the grid points on the shell and solid elements. Freedom to allow for change in beam thickness is accommodated by allowing telescoping at one end of each pair of RBAR's, shown in Figure 19. The results, given in Figure 20, compare qualitatively to Figure 18 and are considered acceptable.

Case 8 - Because of the lack of telescoping on the upper end of each pair of RBAR's in Case 7, all load in the z direction is transferred from the shell to only the upper grid point on the HEXA element. This condition is alleviated by allowing telescoping at both ends of each pair of RBAR's. Displacement in the z direction of the shell element is forced to be the average of the HEXA corner displacements by multipoint constraint equations. This forces z direction load to be distributed to both HEXA corner grid points. The interface model is shown in Figure 21; the results are shown in Figure 22. No significant improvement occurs over Case 7, and the complication of distributing z load is not considered worthwhile.

Case 9 - In a manner similar to that in Case 6, RBE3 rigid elements are introduced at the interface. The interface model is shown in Figure 23. Results shown in Figure 24 compare reasonably with the baseline in Figure 18. This alternative is considered acceptable for interfacing between QUAD4 and 8-node HEXA elements. It is interesting to note that the results of Cases 8 and 9 are identical. The reason is that only two grid points are used to determine the least square weighted average displacements and rotations of the reference grid point on the RBE3 elements. This yields the same displacements and rotations as the forced linear variation of Case 8.

2.2.5 QUAD8 to 20-Node HEXA Interface - The H20Q8 model used for interfacing QUAD8 and 20-node HEXA elements is illustrated in Figure 4E. Like the H8Q4 model, a change in the order of the shell and solid elements is not involved, and the interface is relatively simple.

Case 10 - The interface for this case is shown in Figure 25. The RBAR's at the corners of the HEXA element are configured similarly to Case 2. Additional RBAR's are introduced at the center of the beam to enforce compatible displacement and transfer moments. All RBAR's are allowed to telescope except the upper center. Force in the z direction is transferred only to the middle edge grid point at the corners of the solid element (7 and 8). The z direction force from the center grid point of the shell is transferred to only one, 21, of the HEXA edge grid points. The results, shown in Figure 26, contain acceptable perturbation to stresses at the interface.

Case 11 - RBE3 rigid elements similar to Case 6 are used. Grid points occupying the same spatial position are given separate identities for the QUAD8 and HEXA elements. Figure 27 shows the interface configuration. Figure 28 shows the perturbation to stresses to be acceptable under bending loads. As in Case 6, there is more perturbation to σ_{zx} under axial load with RBE3 elements than with RBAR's.

3. PLATE-BENDING VERIFICATION MODEL

The alternative methods of modeling the shell solid interface found acceptable in Section 2 are now introduced into a more complex model. A 1/4 by 10 by 14 in. rectangular aluminum plate subjected to a uniform pressure load of 50 psi is used. The edges of the plate are simply supported. The plate verification problem is shown in Figure 29. Note that the boundary condition of normal displacement $w = 0$ at $x = 0$, $x = 14$, $y = 0$, $y = 10$ also implies that $\frac{\partial w}{\partial x} = 0$ at $y = 0$ and $y = 10$, and $\frac{\partial w}{\partial y} = 0$ at $x = 0$ and $x = 14$. The coordinate system for reporting stresses is the same as the basic system of Figure 29.

3.1 Theoretical Solution - A series solution for normal displacement of the above problem is found in Reference 1. The normal displacement w is given by:

$$w = \frac{16p}{\pi^6 D} \sum_{m=1}^{\infty} \sum_{n=1}^{\infty} \frac{\sin\left(\frac{m\pi x}{a}\right) \sin\left(\frac{n\pi y}{b}\right)}{mn\left(\frac{m^2}{a^2} + \frac{n^2}{b^2}\right)} \qquad m,n = 1,3,5 \ldots$$

where D is the plate flexural rigidity defined as:

$$D = Et^3/12\,(1 - \nu^2)$$

This series is differentiated to find the bending and twisting moments per unit length by:

$$M_x = -D\left(\frac{\partial^2 w}{\partial x^2} + \nu \frac{\partial^2 w}{\partial y^2}\right)$$

$$M_y = -D\left(\frac{\partial^2 w}{\partial y^2} + \nu \frac{\partial^2 w}{\partial x^2}\right)$$

$$M_{xy} = D\left(1 - \nu\right) \frac{\partial^2 w}{\partial x \partial y}$$

These are converted to normal and shear stresses on the upper surface by:

$$\sigma_{xx} = 6M_x/t^2$$

$$\sigma_{yy} = 6M_y/t^2$$

$$\sigma_{xy} = -6M_{xy}/t^2$$

The transverse running shear forces are given by:

$$Q_x = -D \frac{\partial}{\partial x}\left(\frac{\partial^2 w}{\partial x^2} + \frac{\partial^2 w}{\partial y^2}\right)$$

$$Q_y = -D \frac{\partial}{\partial y}\left(\frac{\partial^2 w}{\partial x^2} + \frac{\partial^2 w}{\partial y^2}\right)$$

Conversion to average transverse shear stress is accomplished by:

$$\sigma_{zx} = Q_x/t$$

$$\sigma_{yz} = Q_y/t$$

The above expressions for stresses were incorporated into a Fortran program with sufficiently high values for m and n to provide for accurate convergence. The stress expressions were evaluated along the line y = 1, where the shell/solid interface occurs in the finite element models. The series summation from the Fortran program provides the theoretical values against which the finite element model results are compared in the following cases.

3.2 Finite Element Models - All finite element models represent one quarter of the 10 x 14 plate, using planes of symmetry at y = 5 and x = 7. The modeled quadrant is shown in Figure 29. Elements, whether shell or solid, are one-inch squares in the xy plane. Wherever solid and shell elements are both used in the plate model, the shell elements occupy the region y > 1; and solids, y < 1. Interfaces between 20-node HEXA's and CQUAD4 and 20-node HEXA's and CQUAD8 elements are considered. Loads are distributed through PLOAD bulk data cards for QUAD4 and HEXA elements and by PLOAD4 on QUAD8 elements.

Care is needed to ensure that single-point constraints used on boundaries of the finite element model are consistent with the mathematical model used by Timoshenko in Reference 1. Referring to Figure 29, they are enumerated. For grid points on shell elements, degrees of freedom 123 are constrained along lines AB and AD; 5 is constrained along AB, and 4 is constrained along AD. 156 are constrained along BC and 246 along CD. All grid points have the shell normal rotation degree of freedom, 6, constrained. For grid points on solid elements, the rotational freedoms 4, 5, and 6 are constrained if not also common to shell elements. Grid points along BC have 1 constrained; along CD, 2 is constrained. Figure 30 illustrates the constraints for grid points on solid elements along planes x = 0 and y = 0. Grid points along AB and AD have displacement freedoms 123 constrained. To enforce the condition of $\frac{\partial w}{\partial y} = 0$ along x = 0, 2 dof is constrained on grid points along $A_u D_u$ and $A_l D_l$. 1 is constrained for grid points along $A_u B_u$ and $A_l B_l$ to enforce $\frac{\partial w}{\partial x} = 0$ on plane y = 0. Multipoint constraint equations are used to force the average of z displacement of edge grid points along lines $A_u B_u$, $A_l B_l$, $A_u D_u$, and $A_l D_l$ to zero without constraining thickness.

3.2.1 Baseline HEXA, QUAI 8, and QUAD4 Models - Results for baseline models composed entirely of HEXA, QUAD8, and QUAD4 are shown in Figures 31, 32, and 33, respectively. Stress values at y = 1.0 reported by neighboring HEXA and QUAD8 elements are averaged for presentation. Stresses for the QUAD4 model are interpolated to determine values at y = 1.0. All models are seen to reasonably approximate the plate theory as described in Section 3.1.

3.2.2 QUAD4 to 20-Node HEXA Interface - The interface methods evaluated in Section 2.2.2 are adapted to the plate-bending model. Referring to Figure 29, 28 QUAD4 elements are used in the model for the region y > 1; seven HEXA elements are used for y < 1. The results of the cantilever beam screening model indicated that the interfaces of Cases 2 and 6 be used in the plate-bending model.

Cases 2 and 6 - RBAR and RBE3 interfaces with deleted midedge nodes described in Cases 2 and 6 as used in Section 2.2.2 are used to interface between QUAD4 and higher-order HEXA elements. The HEXA stress results are averaged at corner grid points and shown by solid symbols in Figures 34 and 35. Results of the QUAD4 elements are extrapolated to determine their values at y = 1.0 and are indicated by hollow symbols. The results are acceptable for the normal stresses and shear stress in the xy plane. However, the transverse shear stresses σ_{zx} reported here on individual elements rather than averaged, are quite high. This method is therefore not regarded as acceptable. The cause of the problem is one of overconstraint; deletion of the upper and lower edge nodes causes the x, y, and z displacements to all vary linearly along the interface. The y displacement degree of freedom is needed to achieve compatibility between the upper and lower surfaces of the shell and HEXA element. The next case is an alternative that enforces linear displacement for only the y degree of freedom.

Case 12 - The RBAR constraint in this case is similar to that in Case 2. The edge nodes at the interface on the upper and lower surfaces of the HEXA element are not deleted. The y displacement degree of freedom only is forced to vary linearly along the upper and lower edges of each element on the interface. This is accomplished with RBE3 elements spanned between the element corner points and shown in Figure 36. Averaged stress results, shown in Figure 37, contain an unacceptable amount of perturbation. Although not shown, as much as ± 4500 psi scatter occurs for σ_{xx} and σ_{yy}. The problem is believed to be caused by the moment M_y from the shell element being converted to force couples in the x direction and concentrated entirely on the corners of the HEXA elements. This condition is improved in the next case.

Case 13 - This case is similar to Case 12, but RBE3 elements are used to force both the x and y displacements to vary linearly along the upper and lower edges. The z direction displacement is maintained independent. Figure 38 illustrates typical constraints for each element. Stress results shown in Figure 39 compare qualitatively to Figure 33 indicating that perturbation from this interface is acceptable.

Case 14 - In this case, RBE3 constraints similar to Case 6 are used on the QUAD4 element corners. Additional RBE3 constraints of the x and y displacements along the upper and lower interface grid points are used, as illustrated on Figure 40. The results of this interface, shown in Figure 41, are qualitatively equivalent to the baseline in Figure 33. Perturbation to stresses is therefore considered acceptable.

3.2.3 QUAD8 and 20-Node HEXA Interface - Referring to Figure 29, the model to test the interface between QUAD8 and 20-node HEXA elements consists of seven HEXA elements in the region $y < 1.0$ and 28 QUAD8 elements for $y > 1.0$. Stress results from the QUAD8 and HEXA elements are averaged at node points.

Case 10 - Results of the RBAR interface of Case 10 as described in Section 2.2.5 are shown in Figure 42. Application of the Case 10 interface is direct since a change in the order of shell and solid elements is not a concern. Qualitative comparison to the baseline QUAD8 results of Figure 32 shows that stresses are as good and perhaps even better with the interfaced shell and solid elements.

Case 11 - The RBE3 interface of Case 11 of Section 2.2.5, when used on the plate-bending model, also shows good results. Case 11 results in Figure 43 compare well with Figure 32 baseline results and are considered acceptable.

4. CONCLUSIONS

In summary, some general conclusions may be reached on methods of introducing an acceptable interface between shell and solid elements. First, kinematic compatibility must be assured so that forces and moments are transferred from shell to solid elements. All cases examined in this paper provide a mechanism for this load transfer. Moments from the shell are introduced into solid elements as force couples through rigid element mechanisms. Second, care must be taken to avoid overconstraint. One example of overconstraint leading to significant perturbation of stress is the rigid plate of Case 4. Another is the restriction of shell thickness in Case 3, which introduces stresses through the Poisson effect. Third, simplicity in application of the interface is a consideration. Seemingly more exact, but also more complex, representations of the interface buy little in the way of improved accuracy in some cases. Case 5 results are nearly identical to Case 2; Case 8 results are nearly identical to Case 7. The difference

between these cases is a simplification which eliminates the multipoint constraint equations at the interface with insignificant loss of accuracy.

The suggested rigid element interfaces, considering kinematic compatibility, accuracy, and simplicity, are relatively straightforward if the order of shells and solids is the same; for example; QUAD8 to 20-node HEXA and QUAD4 to 8-node HEXA. Cases 7 and 9 are suggested methods using RBAR and RBE3 interfaces between QUAD4 and 8-node HEXA elements. Cases 10 and 11 illustrate suggested methods of interfacing QUAD8 and 20-node HEXA elements. Interfaces between QUAD4 and 20-node HEXA elements are more complex. The edge nodes at the upper and lower surfaces on the solid element should allow the displacement normal to the shell to be independent. The other displacement degrees of freedom should vary linearly between the corner grid points on the solid element on the upper and lower edges. Cases 13 and 14 illustrate use of appropriate RBAR and RBE3 interfaces.

It is noted that there is a subtle difference between RBAR and RBE3 elements, applied at the interface. Passing the RBAR elements through points normal to the shell surface ensures they remain normal after deformation. This is consistent with the basic assumption of a thin plate in bending. The RBE3 element does not enforce the condition of normals remaining normal after deformation. It is a matter of the analyst's judgment to decide between the RBAR and RBE3 approach in a particular modeling situation.

5. REFERENCES

Timoshenko and Woinowski-Krieger, Theory of Plates and Shells, McGraw-Hill Book Company, N.Y., 1959, P. 105.

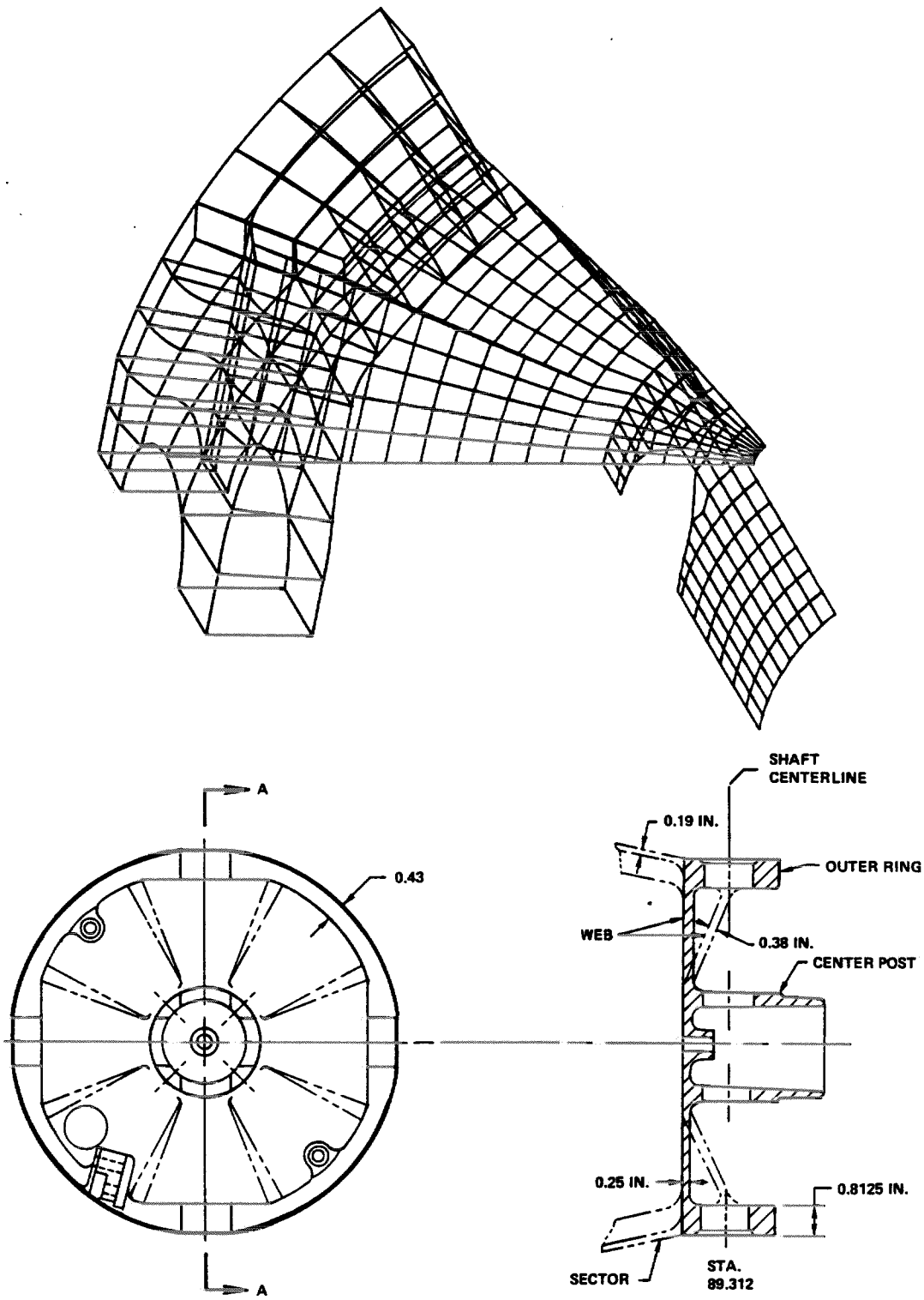

Figure 1 - Aft Bulkhead

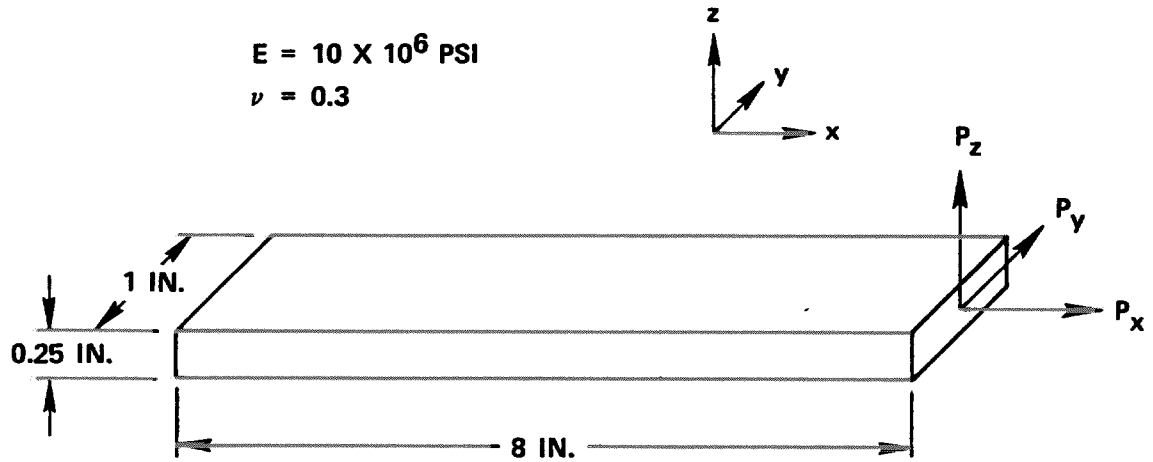

SUBCASE	LOAD (LB)	STRESS AT EXTREME CORNERS	TIP DEFL (IN.)
1	$P_x = 60$	$\sigma_x = 240$ PSI	1.92×10^{-4}
2	$P_y = 60$	$\sigma_x = 11{,}520 - 1{,}440\ x$, $\sigma_{zx} = 240$ PSI	0.0492
3	$P_z = 60$	$\sigma_x = 46{,}080 - 5{,}760\ x$, $\sigma_{yz} = 240$ PSI	0.7864

Figure 2 - Cantilever Beam Properties

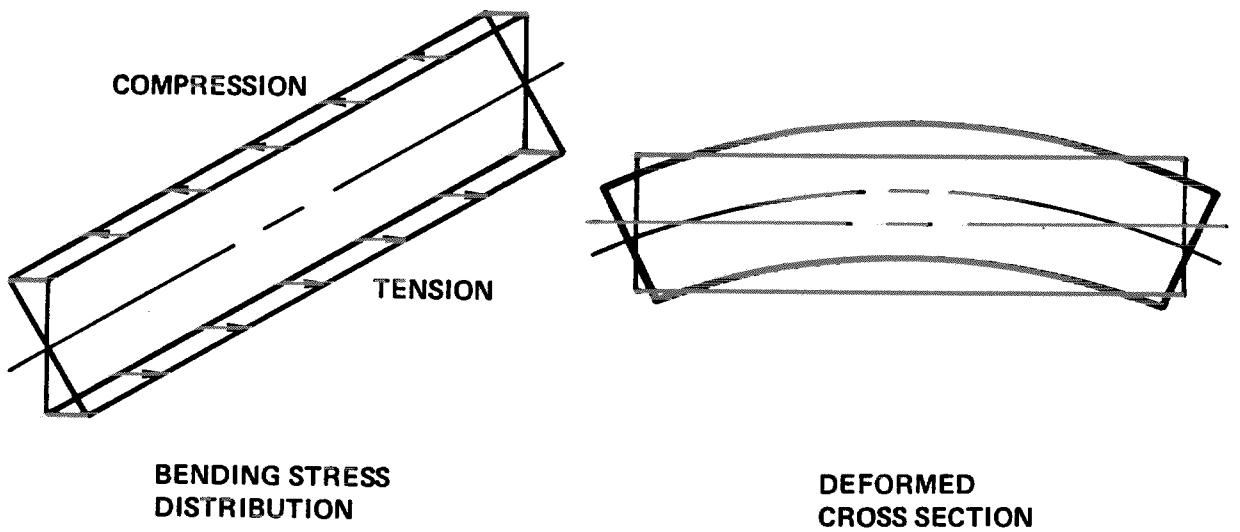

Figure 3 - Beam Cross-Section Deformation

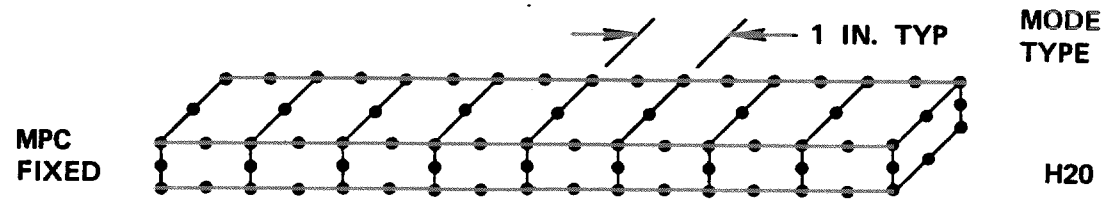

(A) ALL 20-NODE HEXA

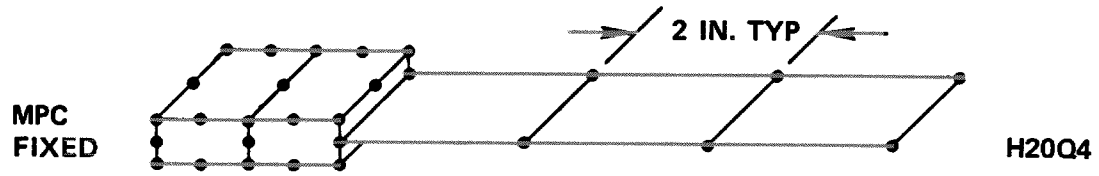

(B) 20-NODE HEXA AND QUAD4

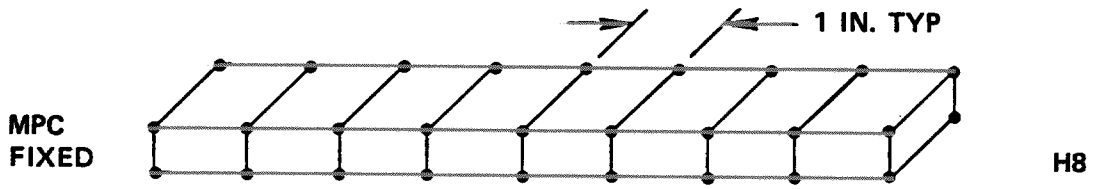

(C) ALL 8-NODE HEXA

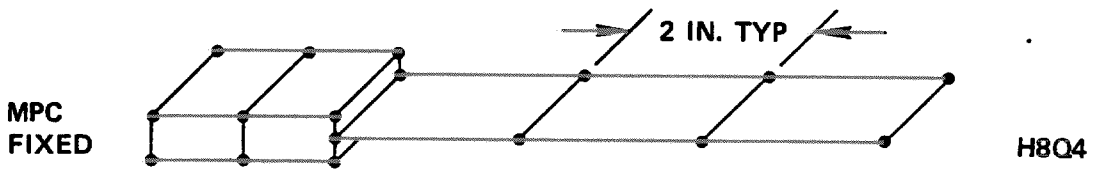

(D) 8-NODE HEXA AND QUAD 4

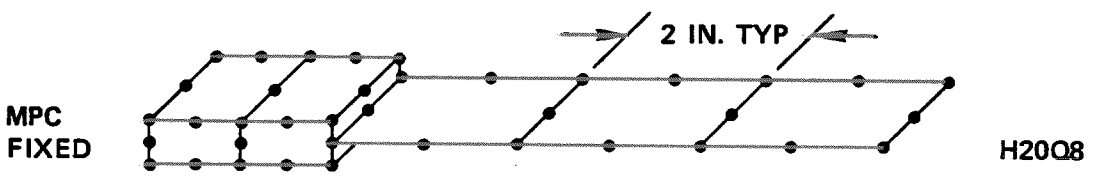

(E) 20-NODE HEXA AND QUAD8

Figure 4 - Beam Finite Element Models

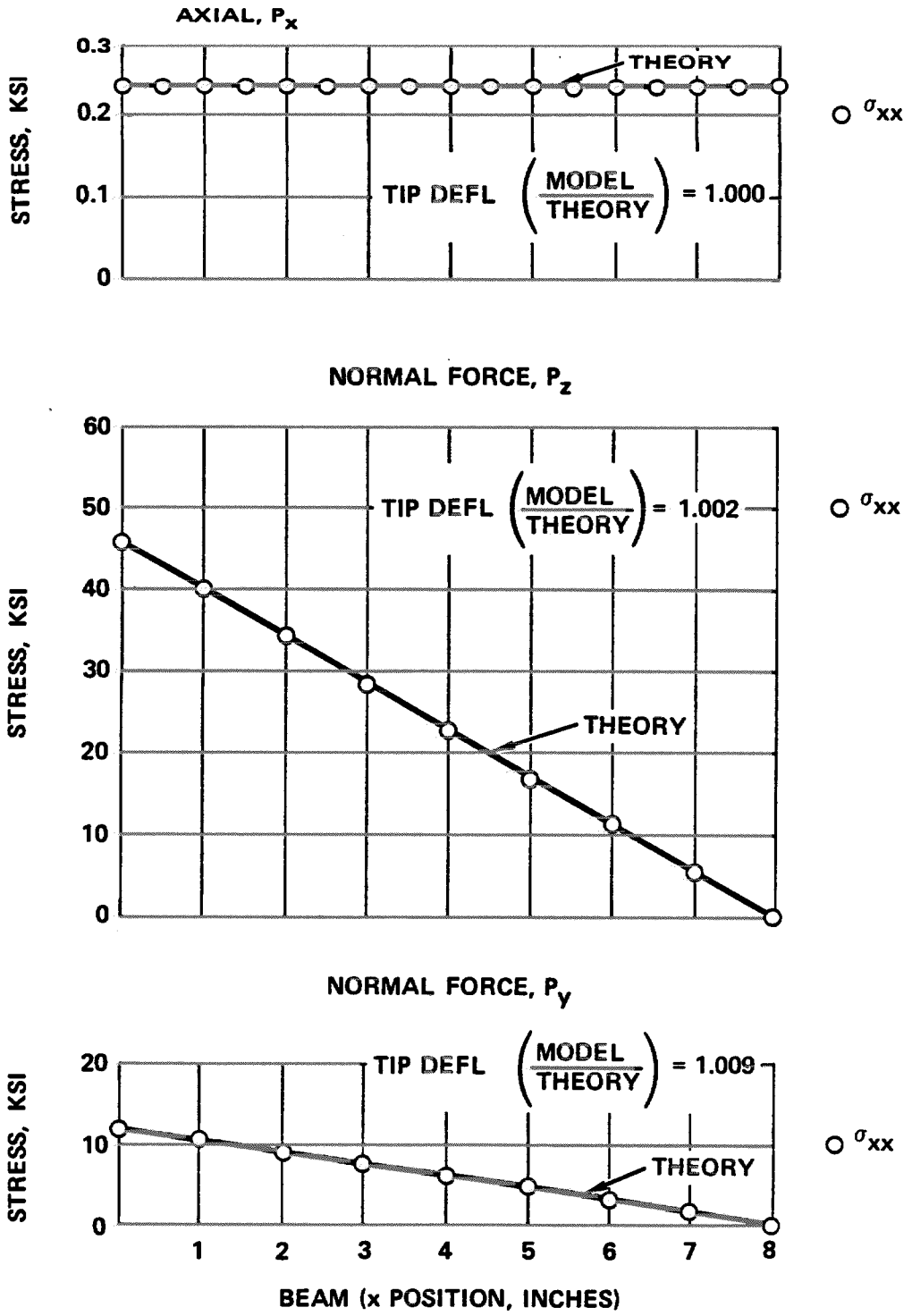

Figure 5 - Baseline Model Results, All 20-Node HEXA Elements

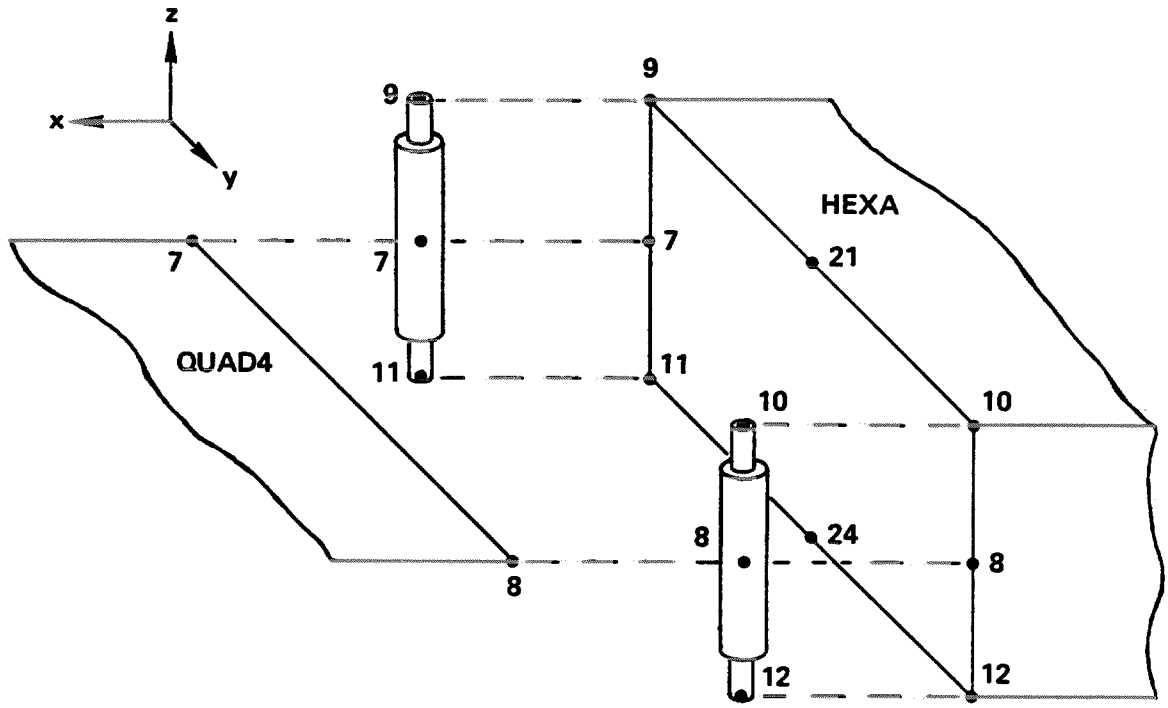

RBAR	EID	GA	GB	CNA	CNB	CMA	CMB		
RBAR	1	7	9	123456			12		
RBAR	2	7	11	123456			12		
RBAR	3	8	10	123456			12		
RBAR	4	8	12	123456			12		

Figure 6 - Case 1 Interface, H20Q4 Model

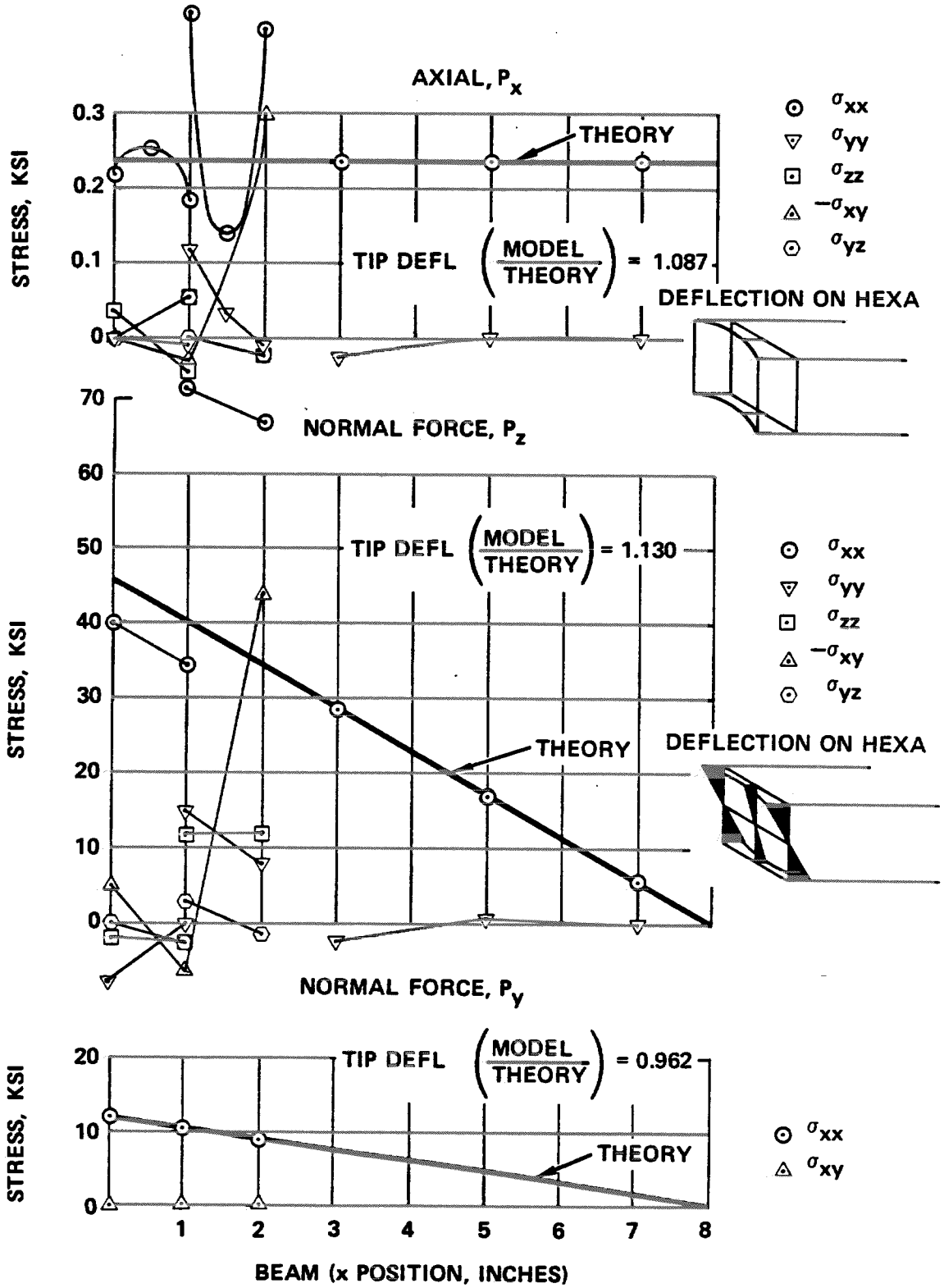

Figure 7 - Case 1 Results, H20Q4 Model

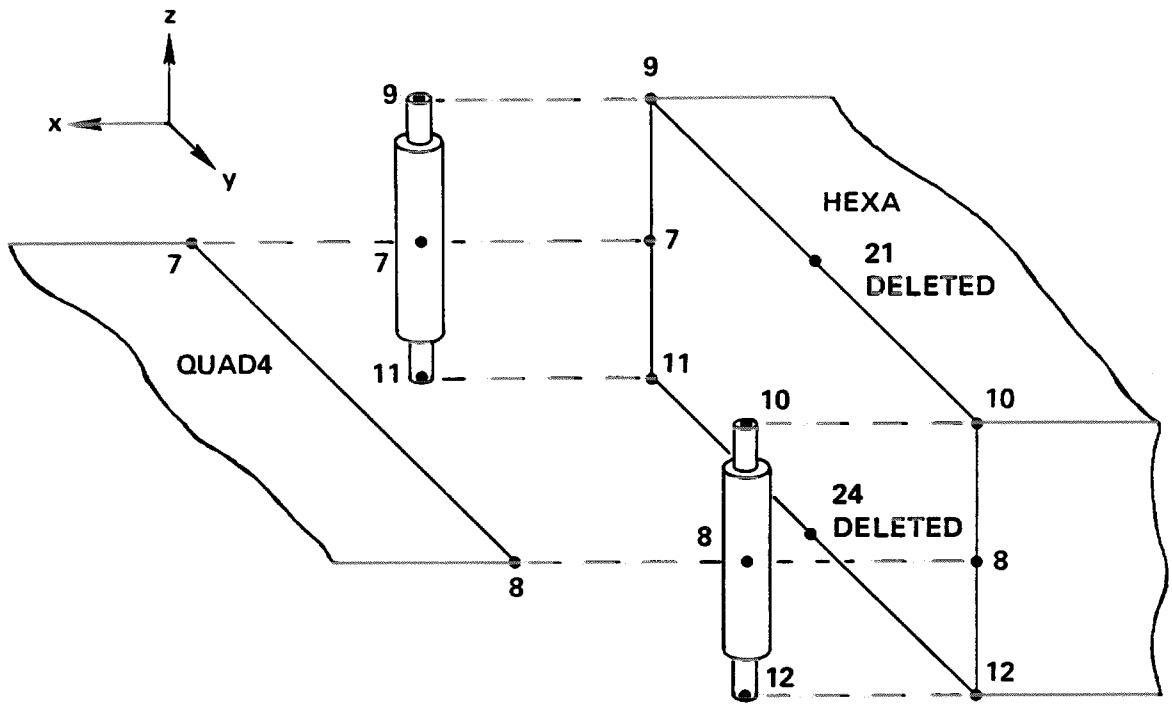

RBAR	EID	GA	GB	CNA	CNB	CMA	CMB		
RBAR	1	7	9	123456			12		
RBAR	2	7	11	123456			12		
RBAR	3	8	10	123456			12		
RBAR	4	8	12	123456			12		

Figure 8 - Case 2 Interface, H20Q4 Model

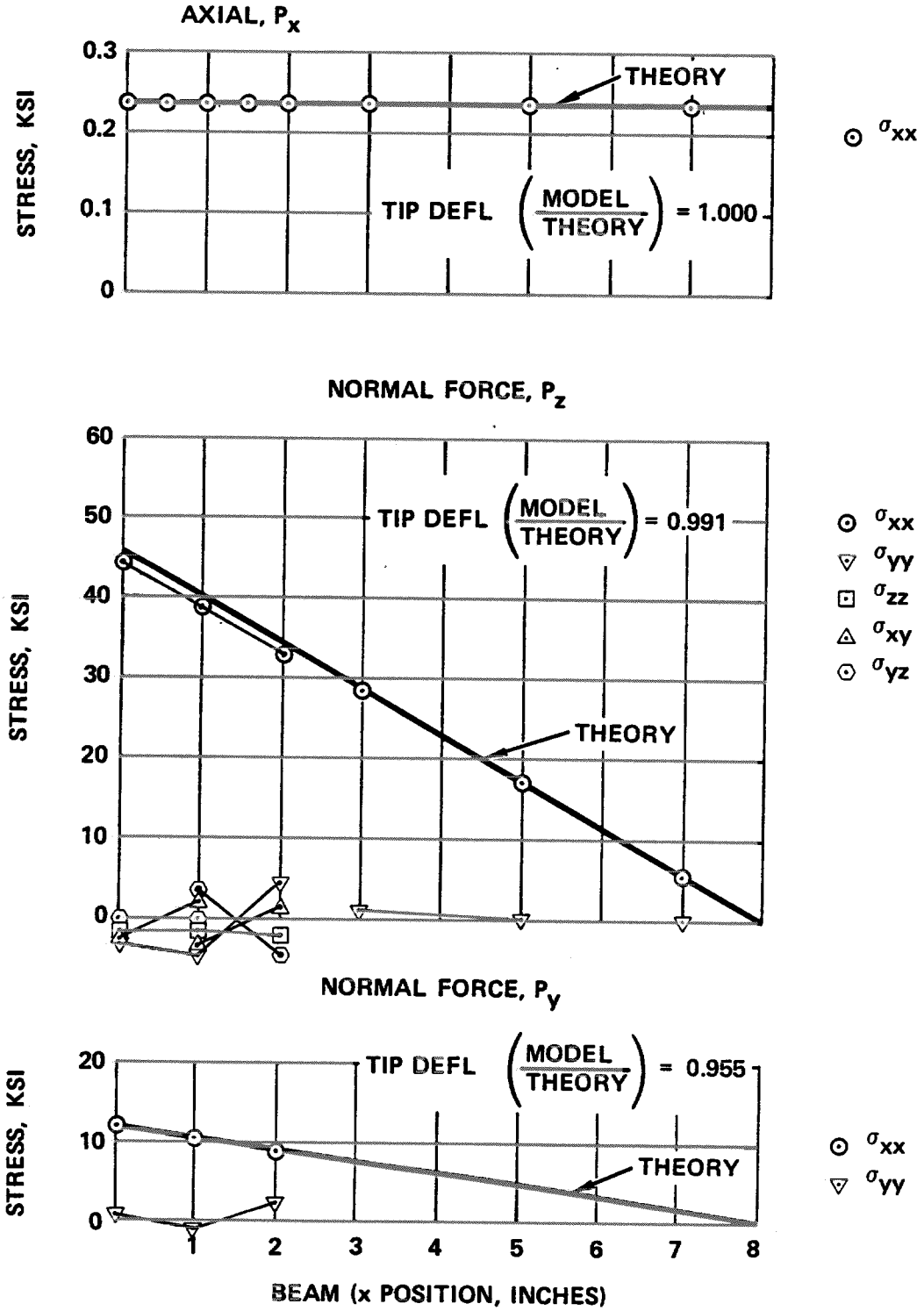

Figure 9 - Case 2 Results, H20Q4 Model

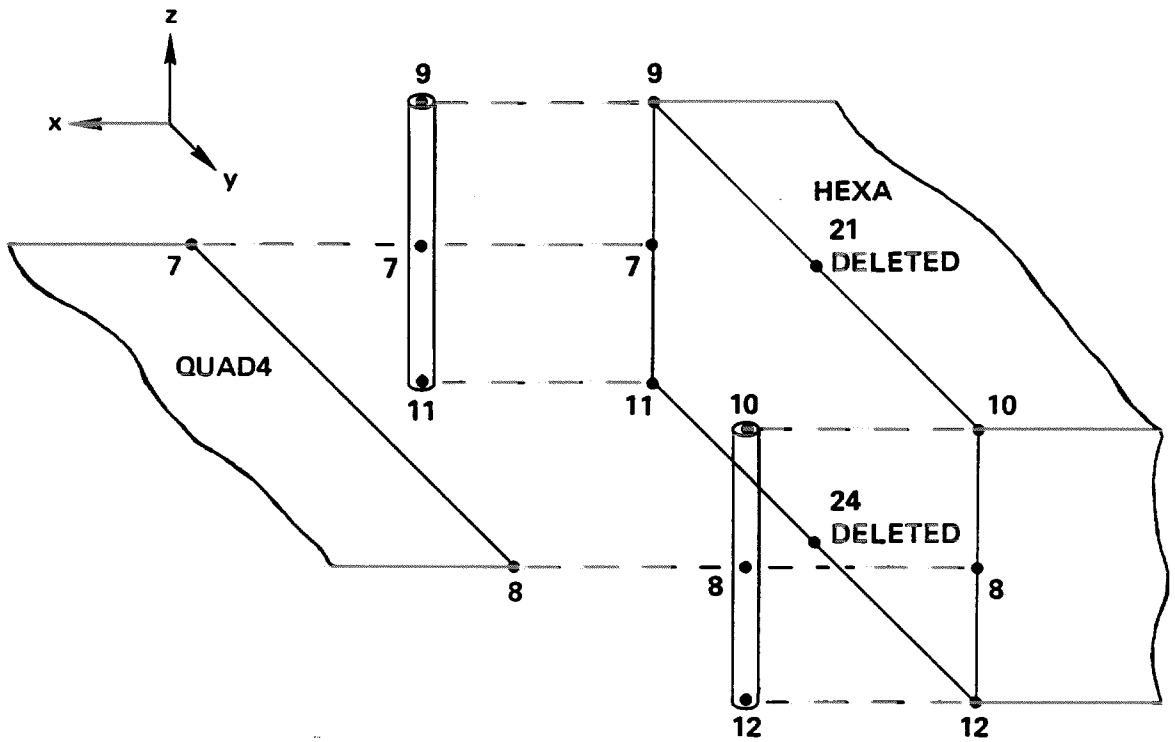

RBAR	EID	GA	GB	CNA	CNB	CMA	CMB		
RBAR	1	7	9	123456			123		
RBAR	2	7	11	123456			123		
RBAR	3	8	10	123456			123		
RBAR	4	8	12	123456			123		

Figure 10 - Case 3 Interface, H20Q4 Model

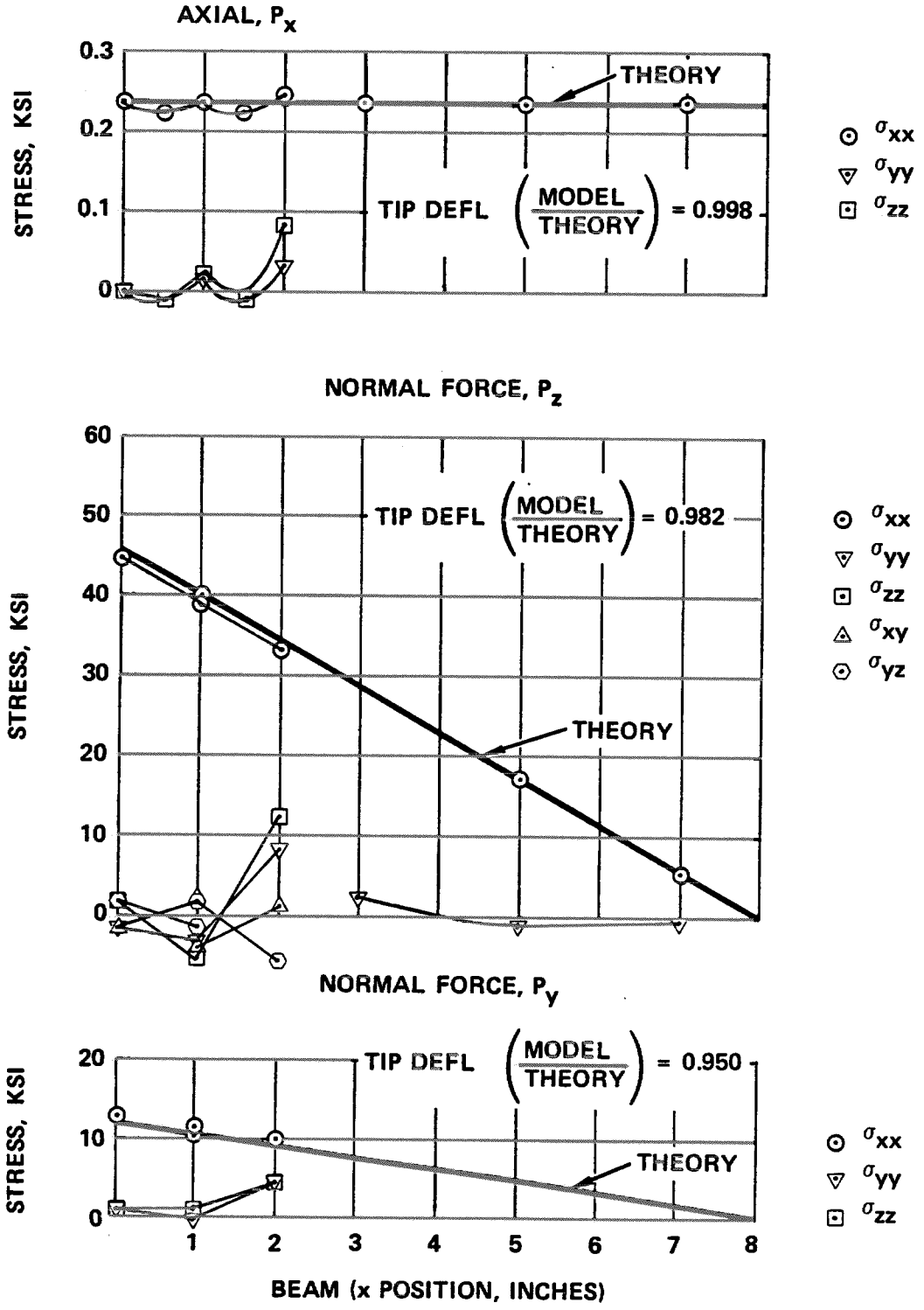

Figure 11 - Case 3 Results, H20Q4 Model

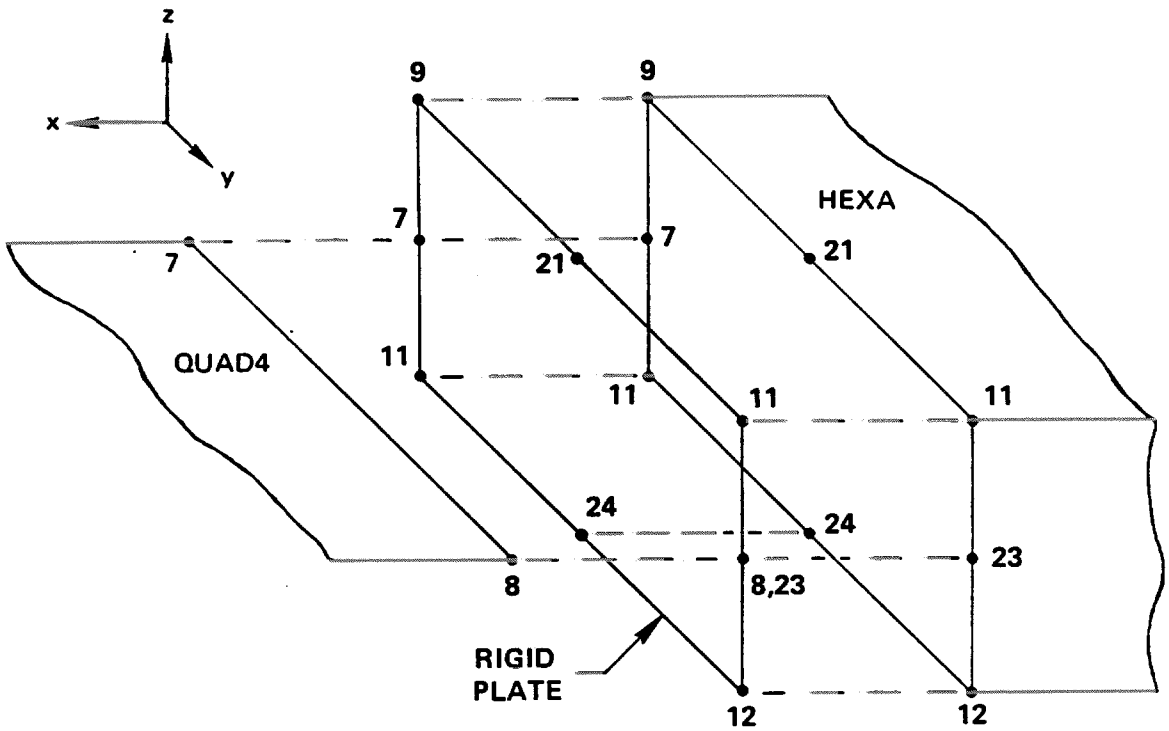

RBE2	EID	GN	CM	GM1	GM2	GM3	GM4	GM5	
RBE2	1	7	123456	8	9	10	11	12	+R1
+R1	21	22	23	24					

Figure 12 - Case 4 Interface, H20Q4 Model

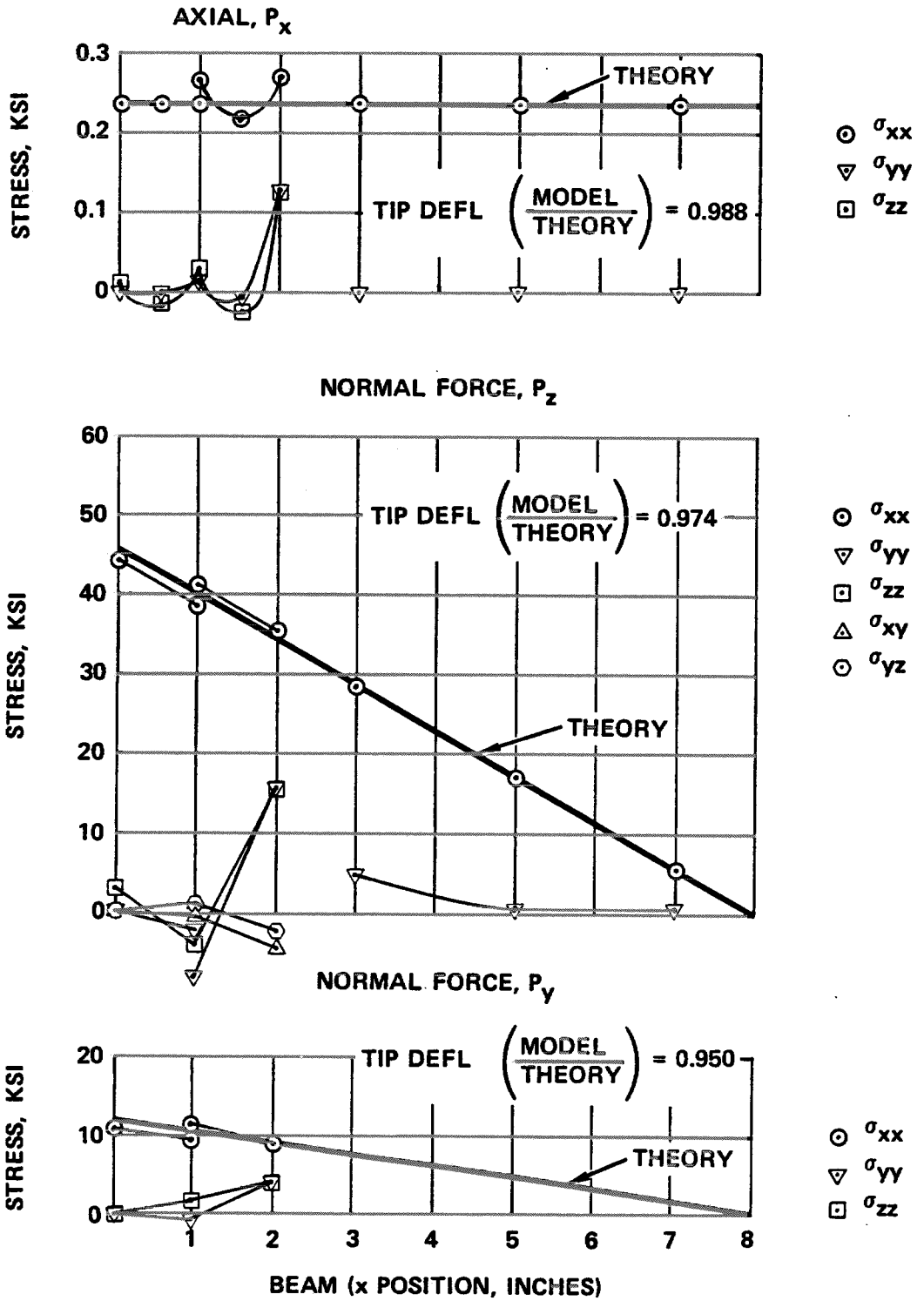

Figure 13 - Case 4 Results, H20Q4 Model

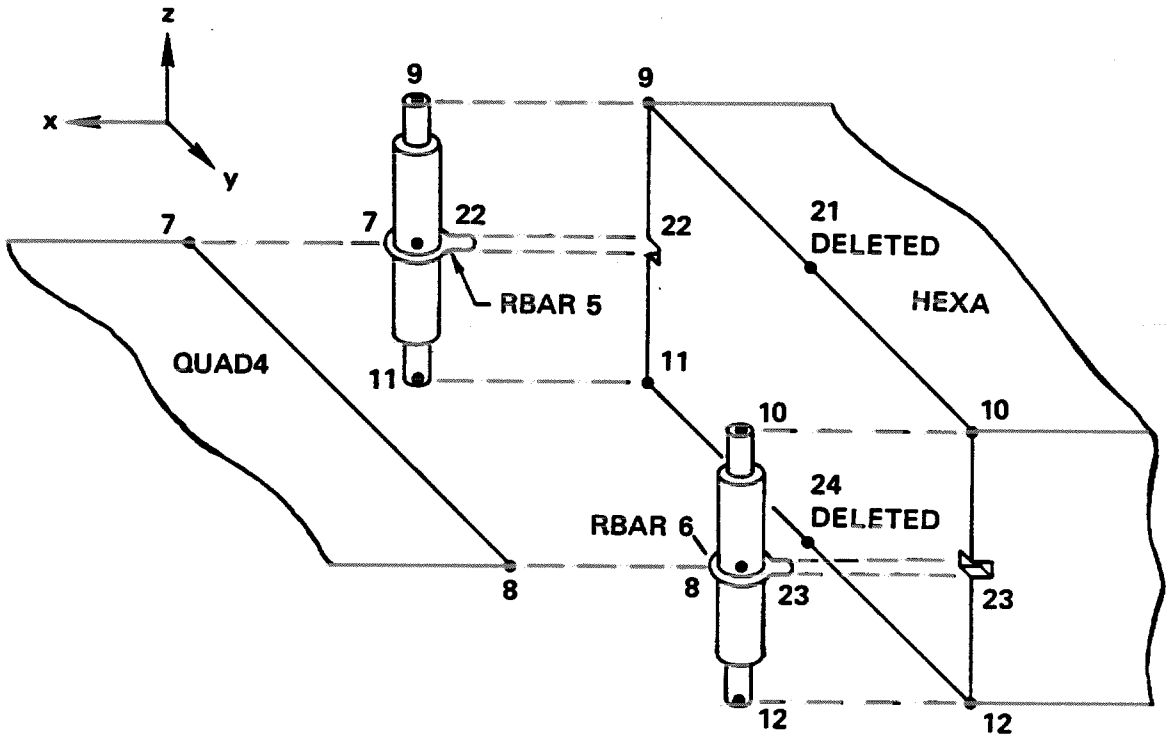

RBAR	EID	GA	GB	CNA	CNB	CMA	CMB		
RBAR	1	7	9	123456			12		
RBAR	2	7	11	123456			12		
RBAR	3	8	10	123456			12		
RBAR	4	8	12	123456			12		
RBAR	5	7	22	123456			12		
RBAR	6	8	23	123456			12		
MPC	SID	G	C	A	G	C	A		
MPC	2	7	3	-3.	9	3	1.		+M1
+M1		22	3	1.	11	3	1.		
MPC	2	8	3	-3.	10	3	1.		+M2
+M2		23	3	1.	12	3	1.		

Figure 14 - Case 5 Interface, H20Q4 Model

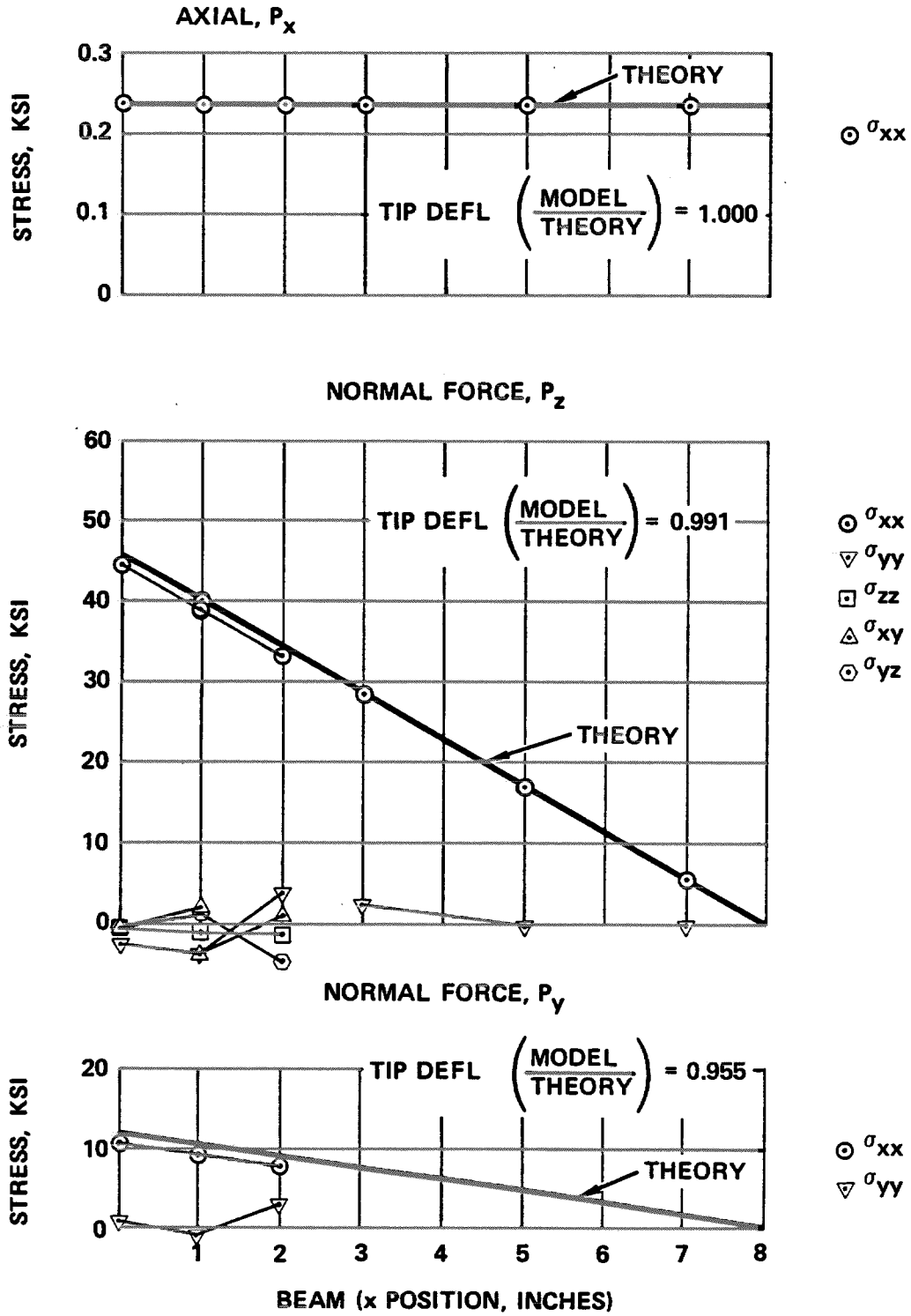

Figure 15 - Case 5 Results, H20Q4 Model

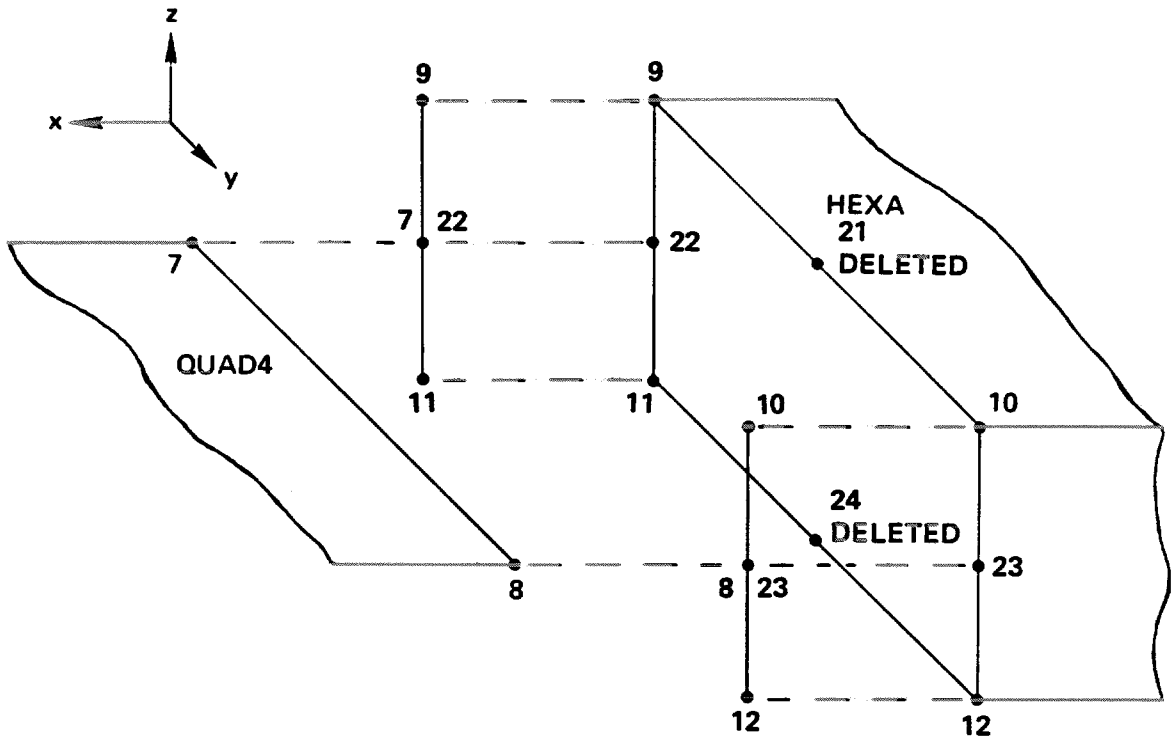

RBE3	EID		REFGRID	REFC	WT1	C1	G1,1	G2,1	
RBE3	10		7	12345	1.	1236	9	11	+RB1
+RB1	22								
RBE3	11		8	12345	1.	1236	10	12	+RB2
+RB2	23								

Figure 16 - Case 6 Interface, H20Q4 Model

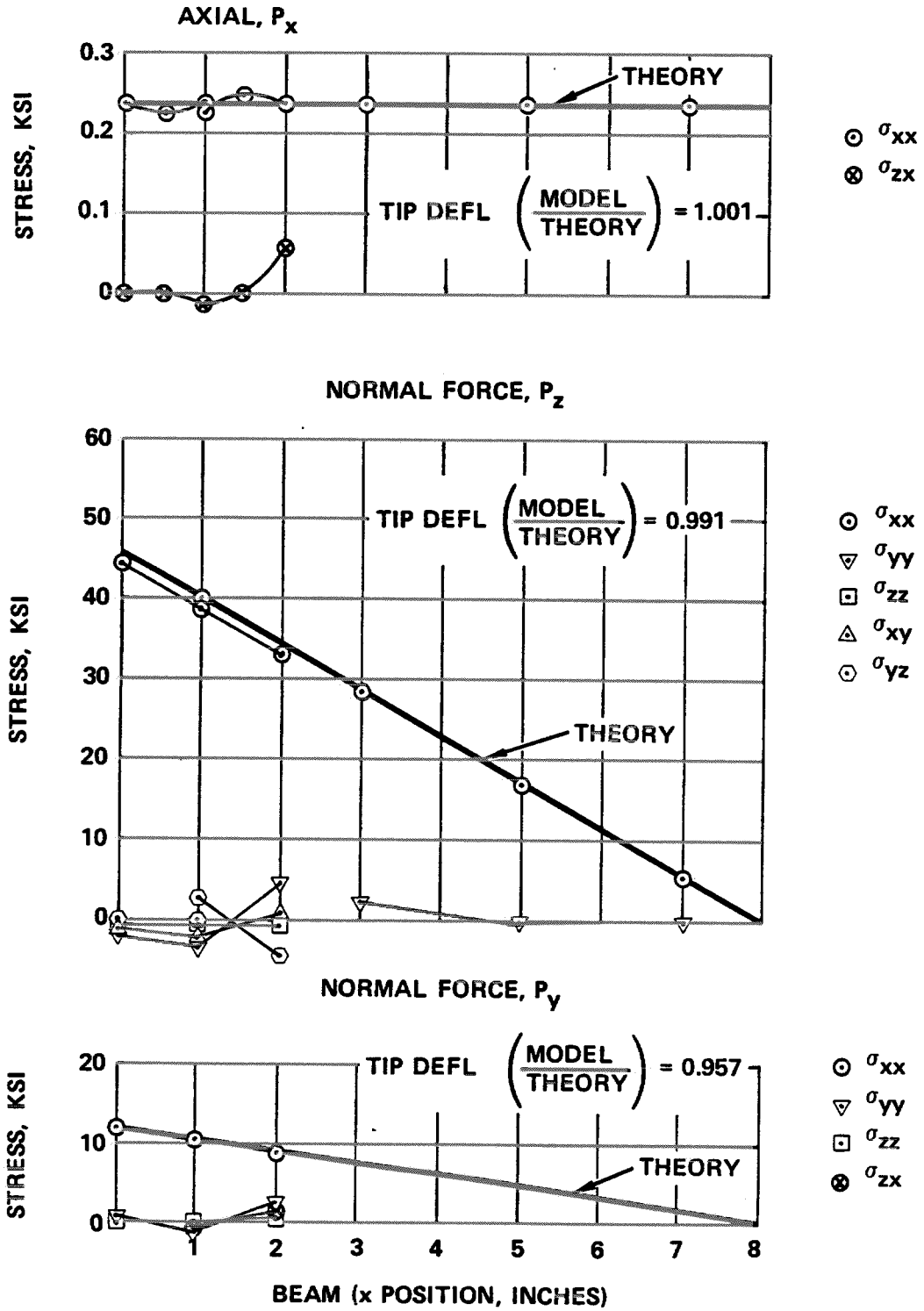

Figure 17 - Case 6 Results, H20Q4 Model

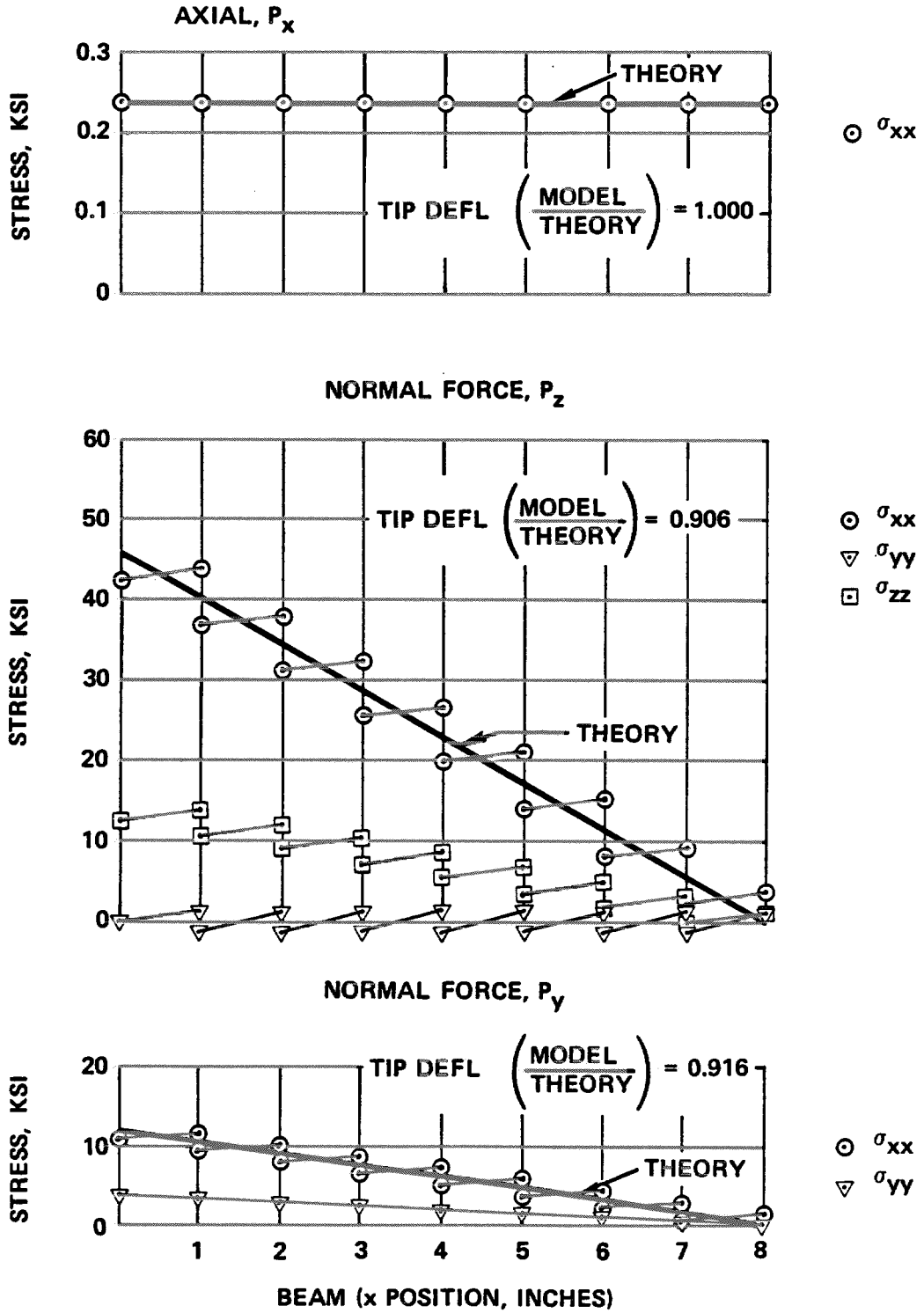

Figure 18 - Baseline Model Results, All 8-Node HEXA Elements

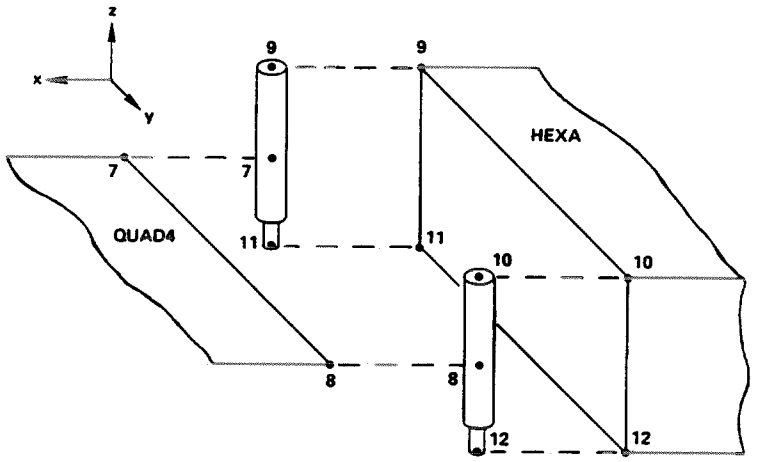

RBAR	EID	GA	GB	CNA	CNB	CMA	CMB		
RBAR	1	7	9	123456			123		
RBAR	2	7	11	123456			12		
RBAR	3	8	10	123456			123		
RBAR	4	8	12	123456			12		

Figure 19 - Case 7 Interface, H8Q4 Model

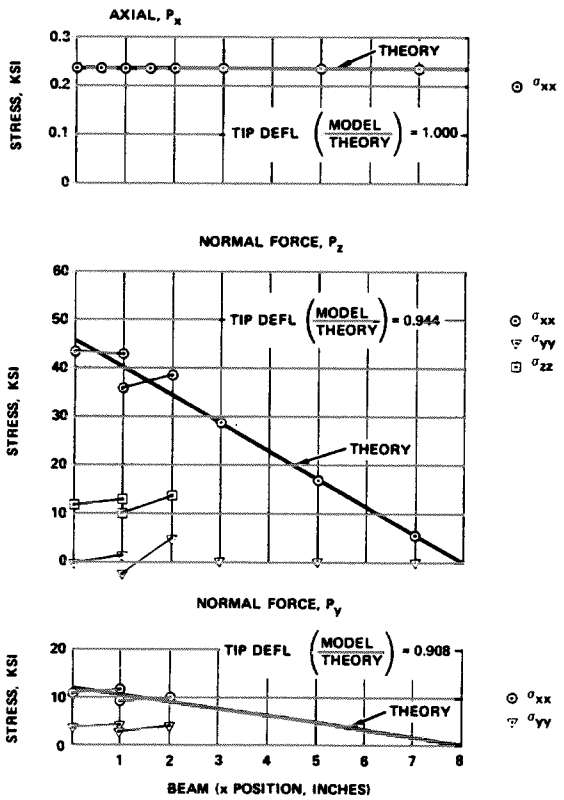

Figure 20 - Case 7 Results, H8Q4 Model

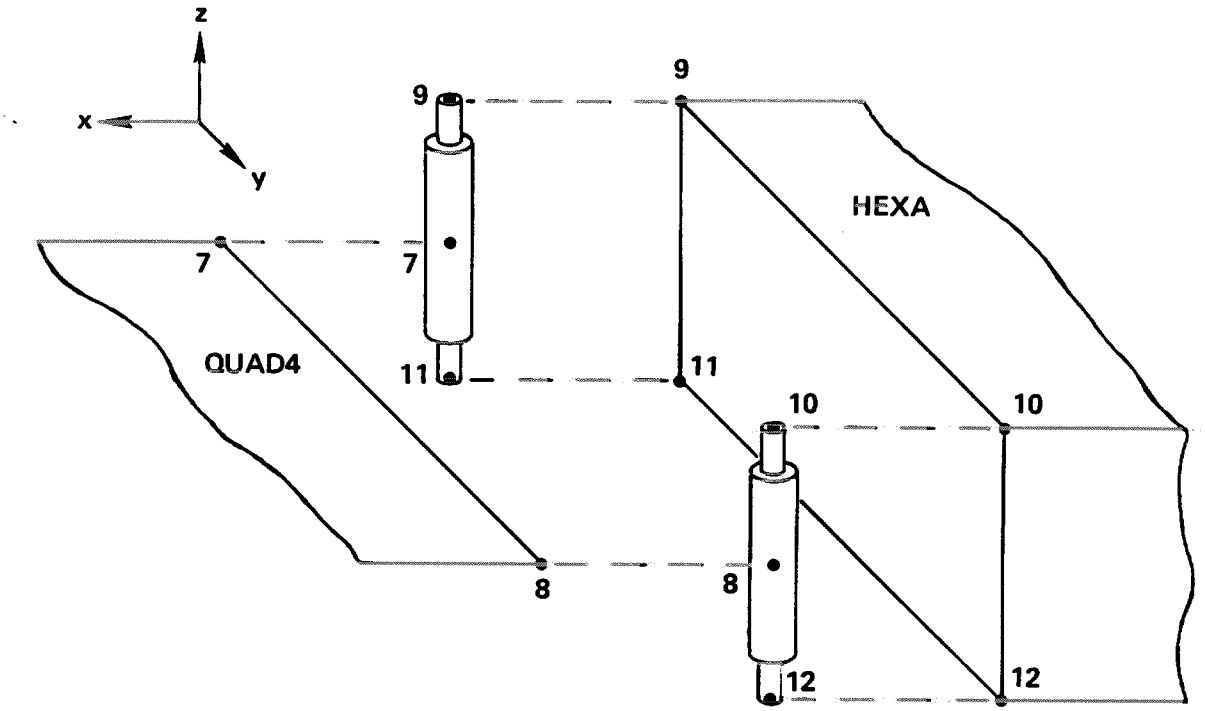

RBAR	EID	GA	GB	CNA	CNB	CMA	CMB		
RBAR	1	7	9	123456			12		
RBAR	2	7	11	123456			12		
RBAR	3	8	10	123456			12		
RBAR	4	8	12	123456			12		

MPC	SID	G	C	A	G	C	A		
MPC	2	7	3	1.	9	3	-.5		+M1
+M1		11	3	-.5					
MPC	2	8	3	1.	10	3	-.5		+M2
+M2		12	3	-.5					

Figure 21 - Case 8 Interface, H8Q4 Model

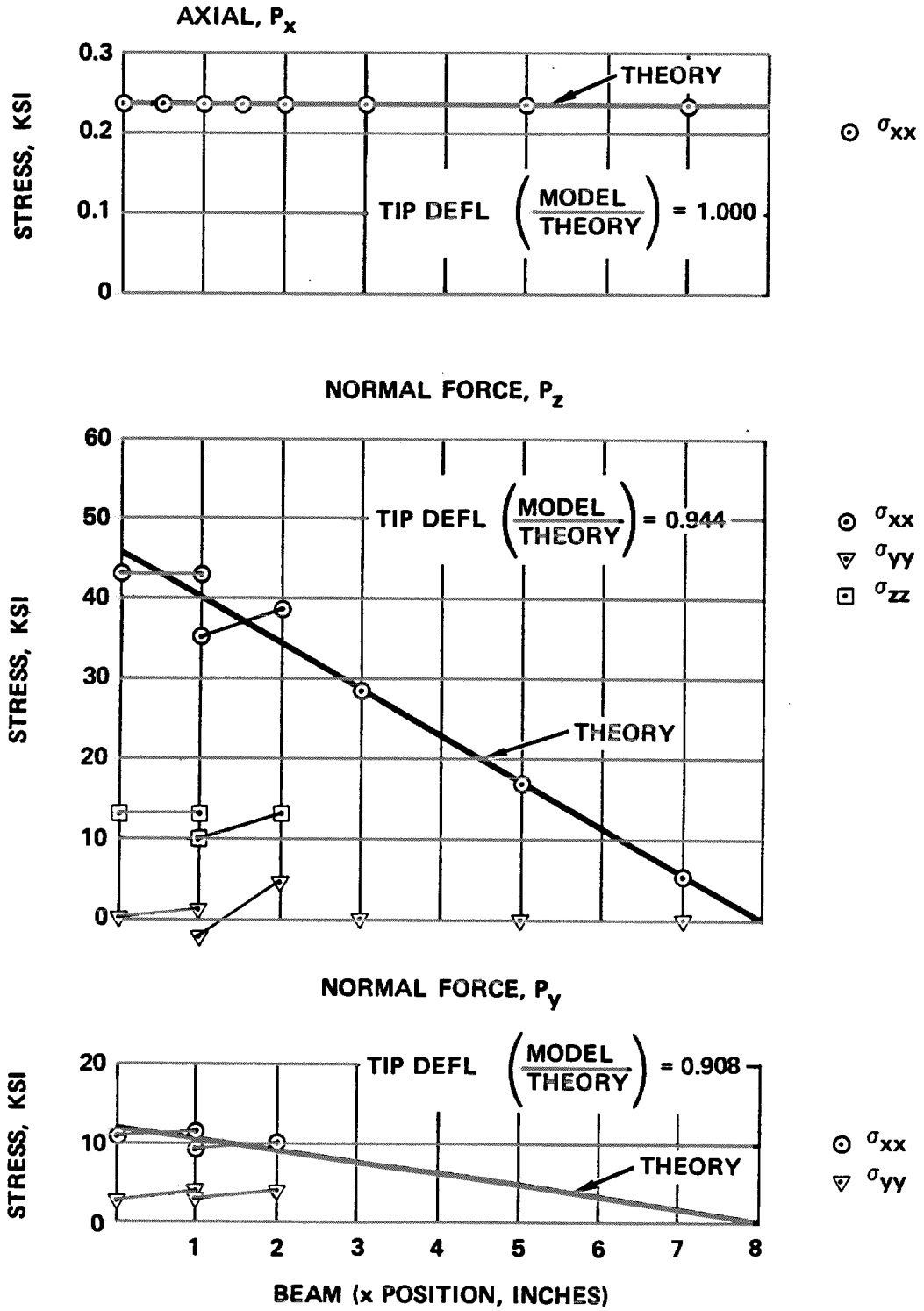

Figure 22 - Case 8 Results, H8Q4 Model

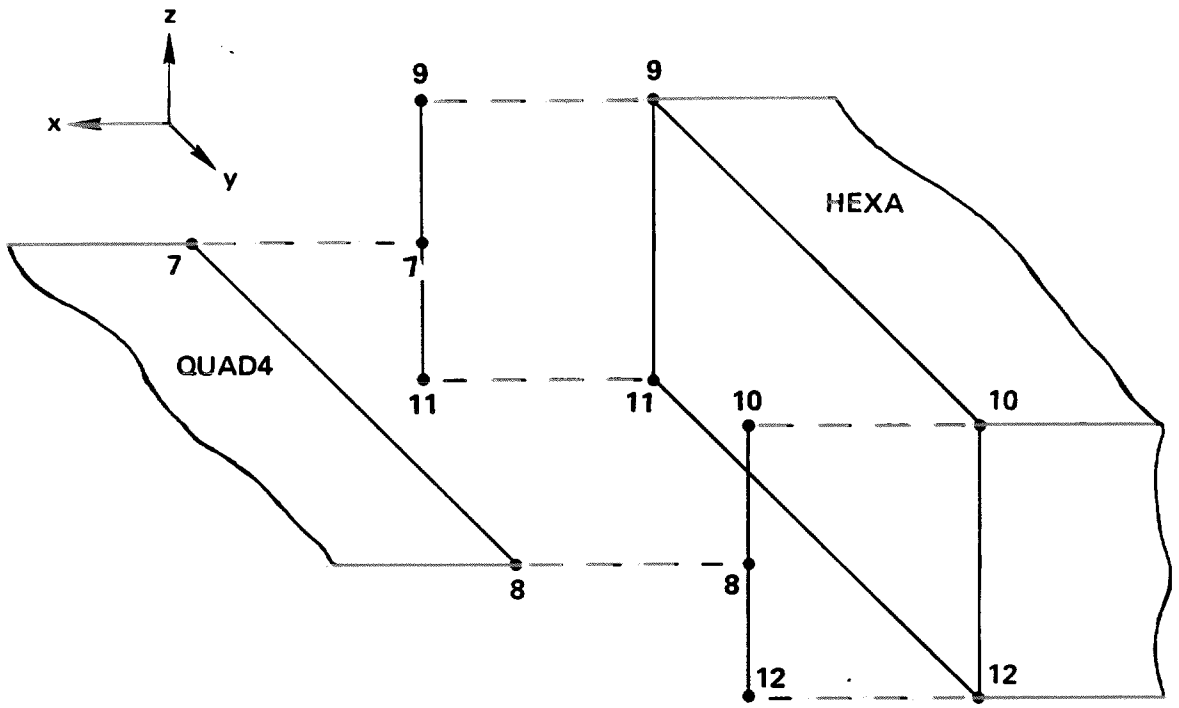

RBE3	EID		REFGRID	REFC	WT1	C1	G1,1	G2,1	
RBE3	1		7	12345	1.	1236	9	11	
RBE3	2		8	12345	1.	1236	10	12	

Figure 23 - Case 9 Interface, H8Q4 Model

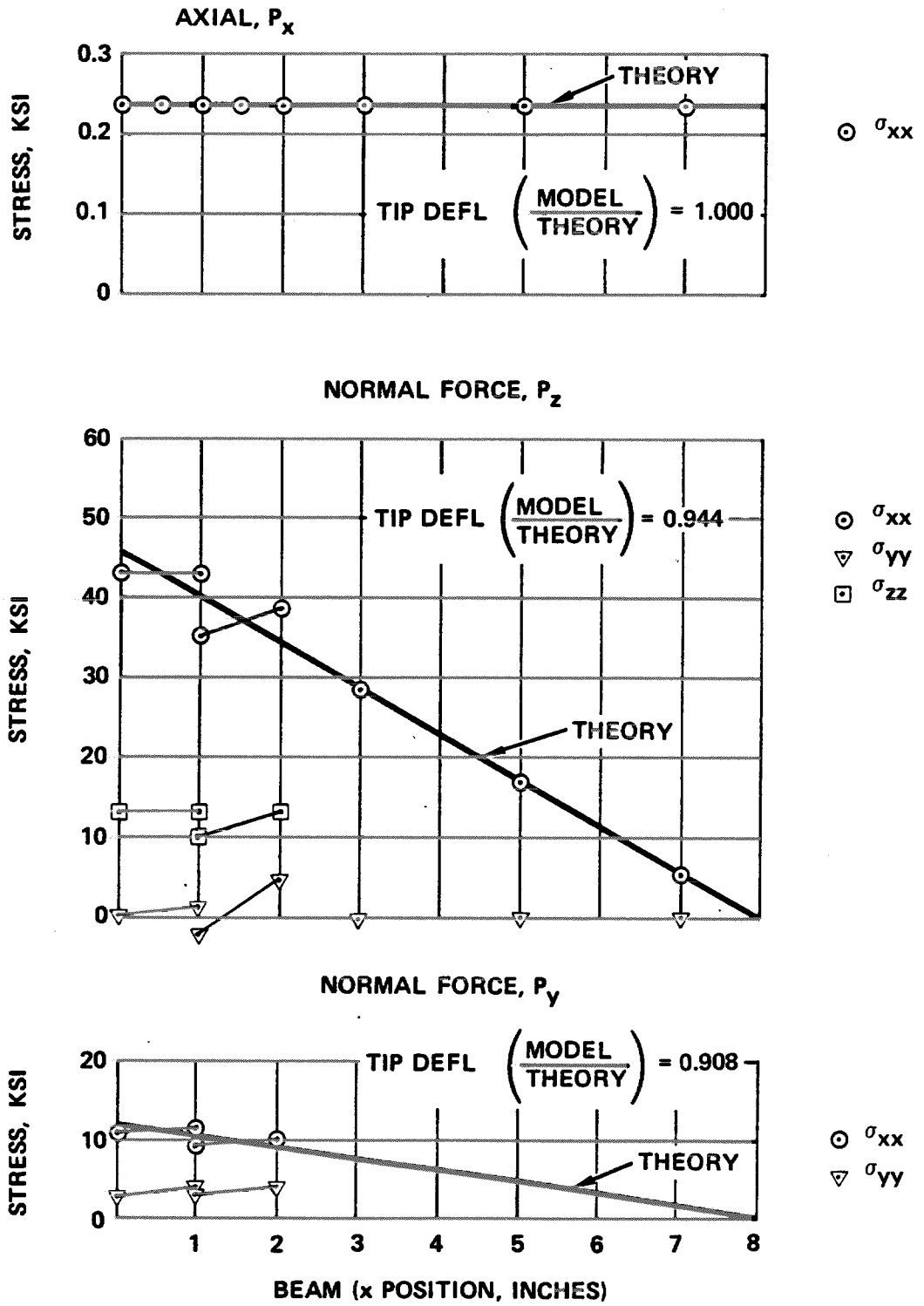

Figure 24 - Case 9 Results, H8Q4 Model

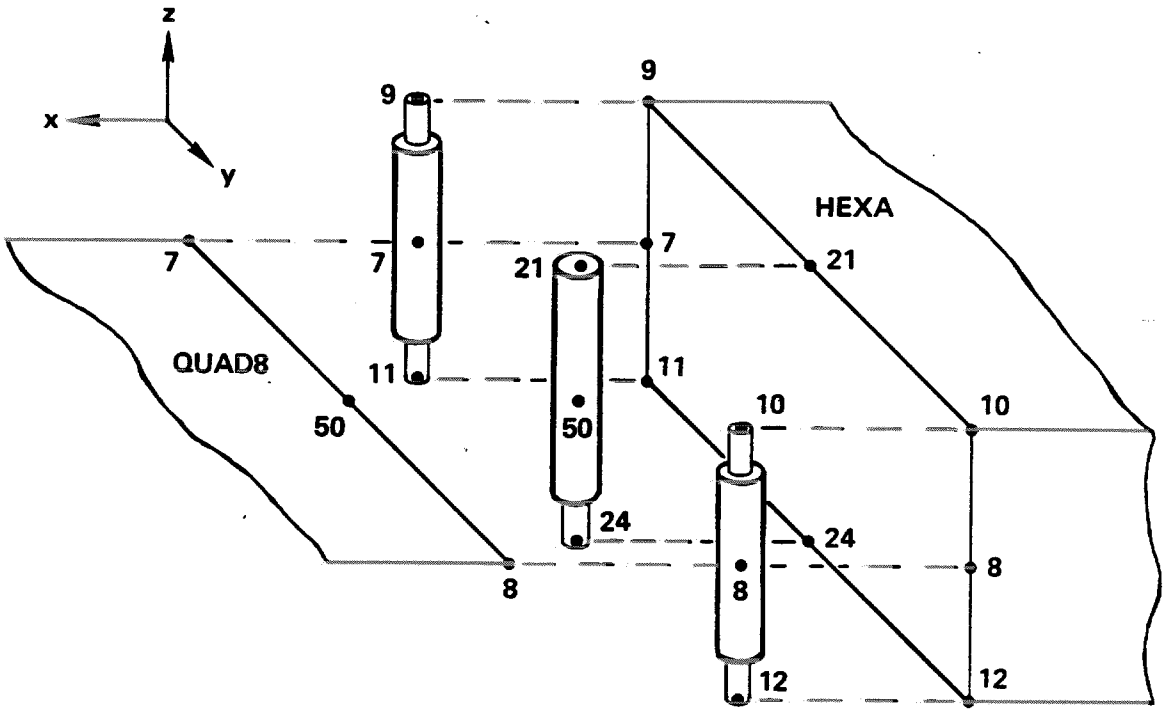

RBAR	EID	GA	GB	CNA	CNB	CMA	CMB		
RBAR	1	7	9	123456			12		
RBAR	2	7	11	123456			12		
RBAR	3	8	10	123456			12		
RBAR	4	8	12	123456			12		
RBAR	5	50	21	123456			123		
RBAR	6	50	24	123456			12		

Figure 25 - Case 10 Interface, H20Q8 Model

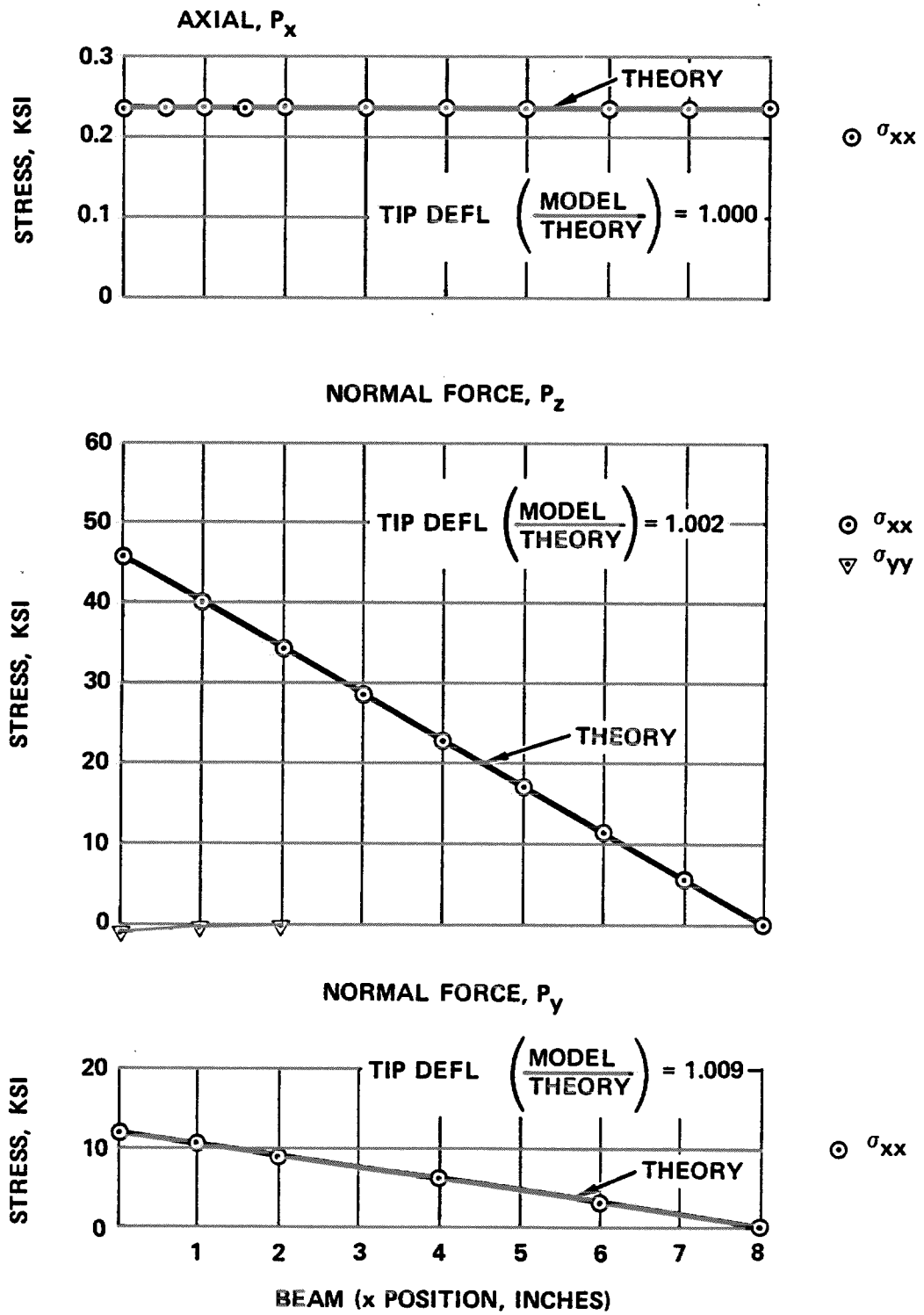

Figure 26 - Case 10 Results, H20Q8 Model

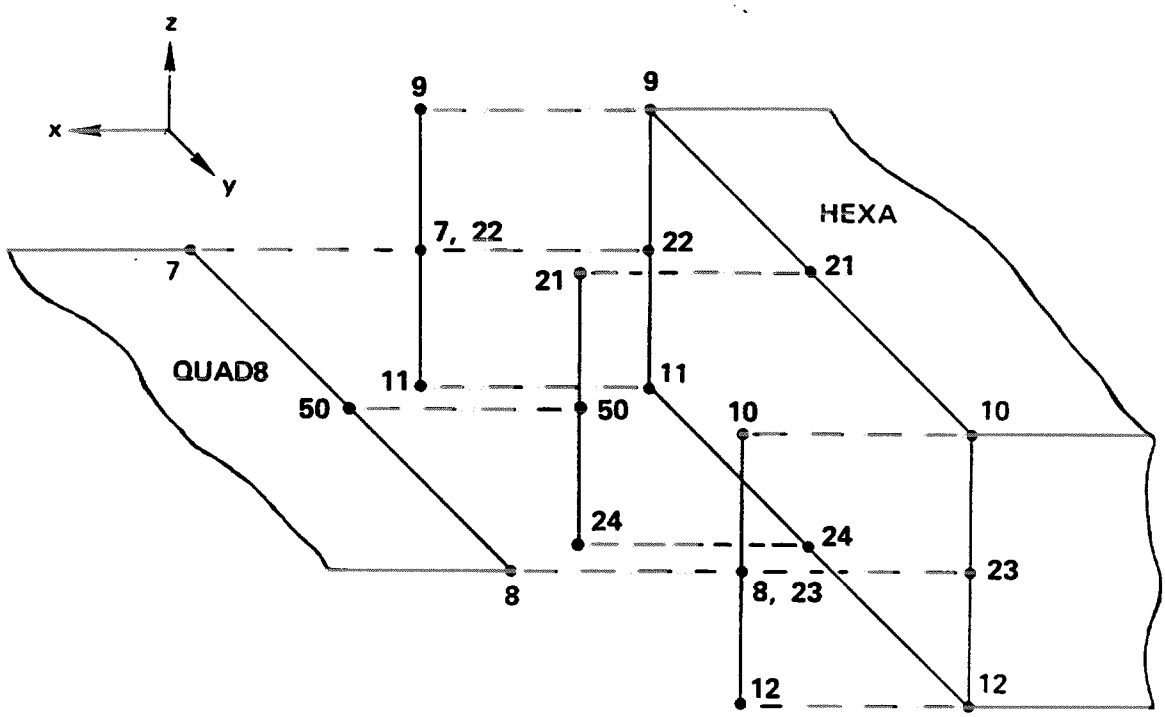

RBE3	EID		REFGRID	REFC	WT1	C1	G1,1	G2,1	
RBE3	1		7	12345	1.	1236	9	11	+RB1
+RB1	22								
RBE3	2		8	12345	1.	1236	10	12	+RB2
+RB2	23								
RBE3	3		50	12345	1.	1236	21	24	

Figure 27 - Case 11 Interface, H20Q8 Model

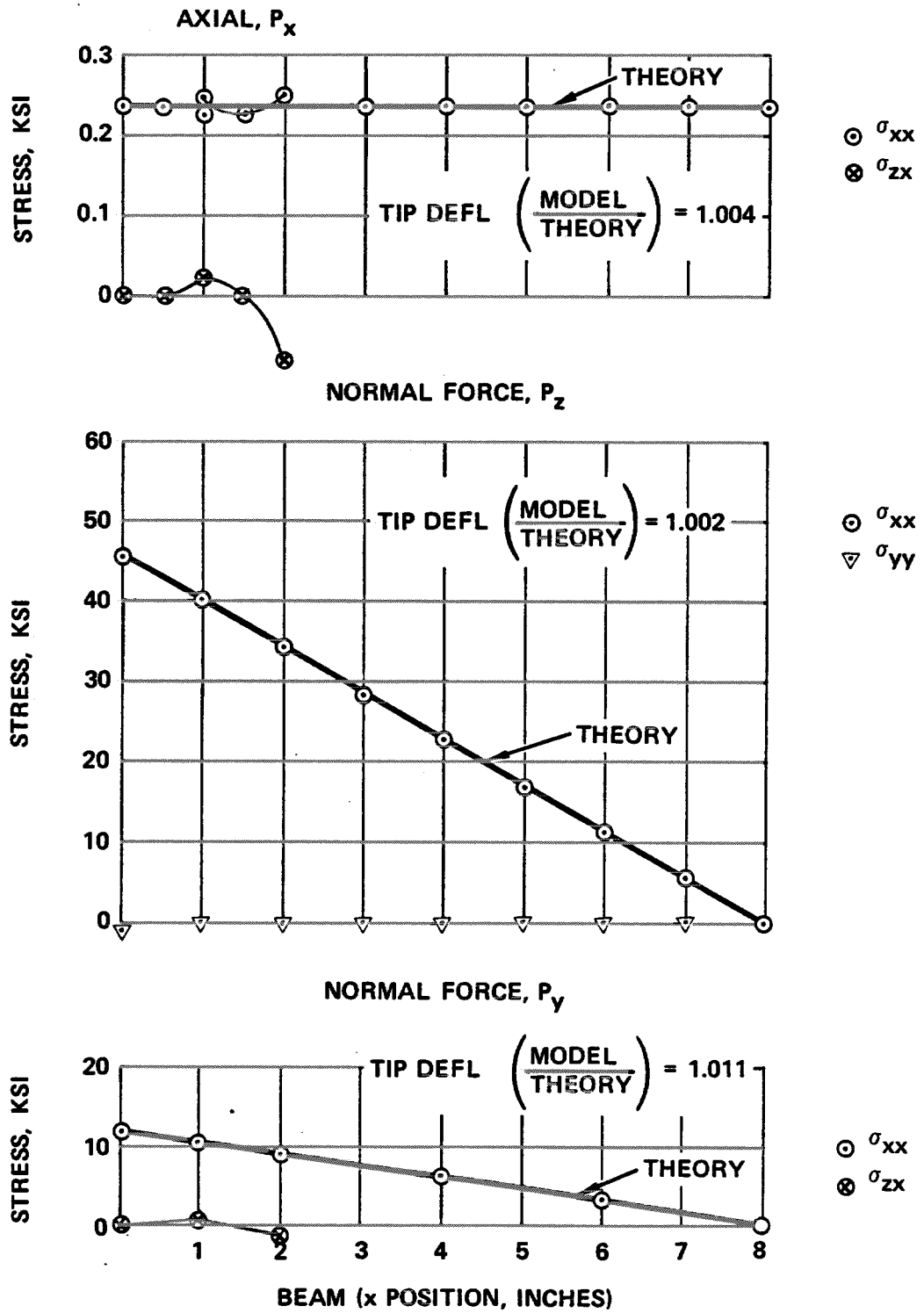

Figure 28 - Case 11 Results, H20Q8 Model

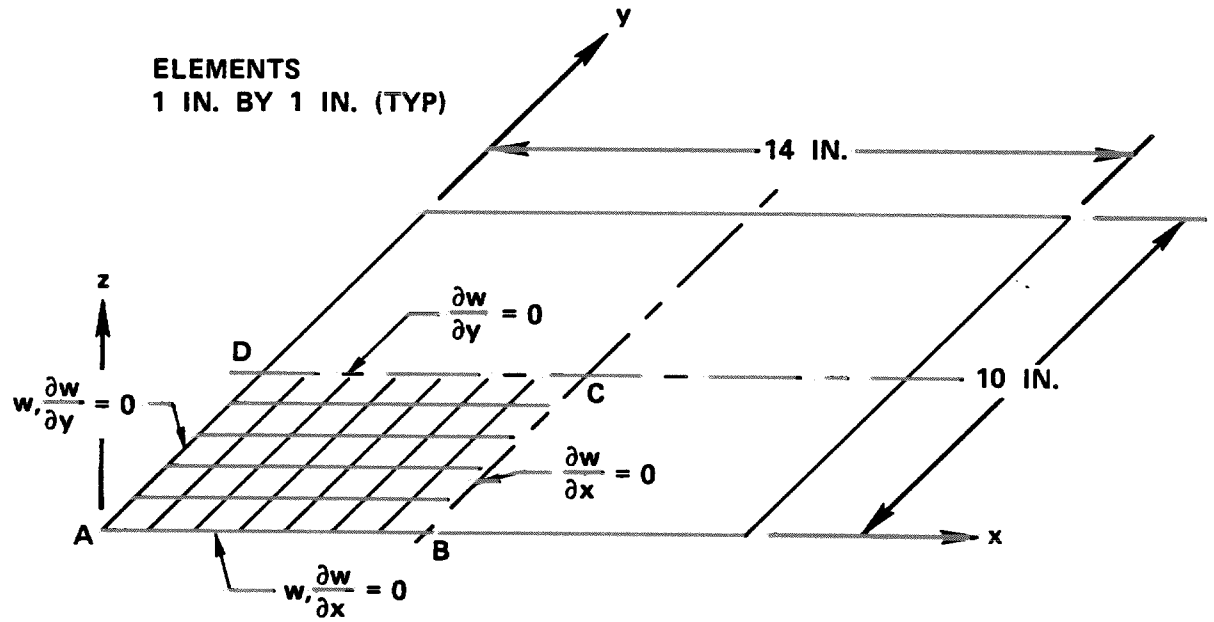

$E = 10^7$ PSI
$\nu = 0.3$
t = 0.25 IN.
p = 50 PSI (IN +z DIRECTION)

Figure 29 - Plate Verification Problem

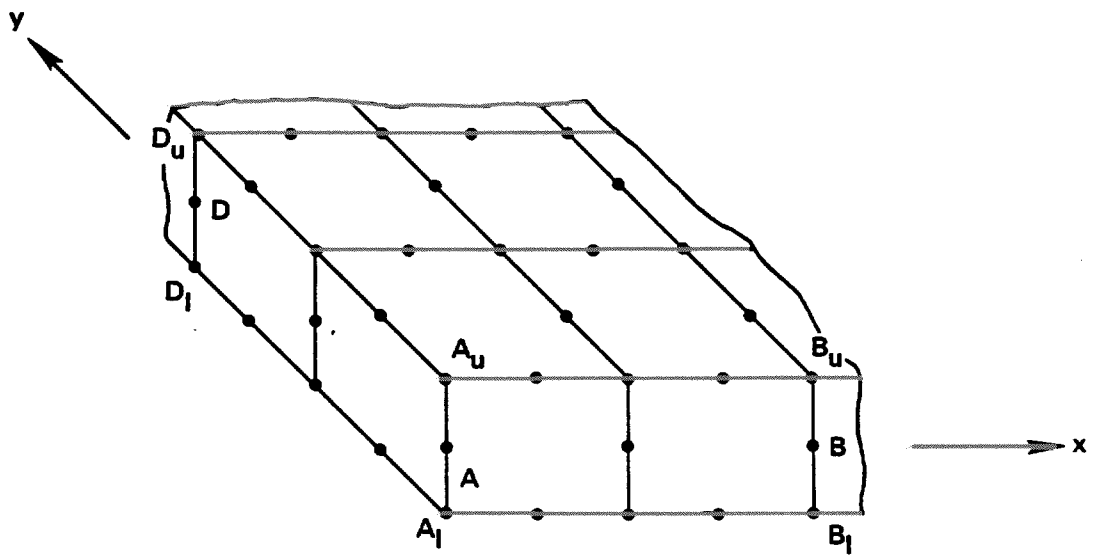

Figure 30 - Simply Supported Edges on HEXA Elements

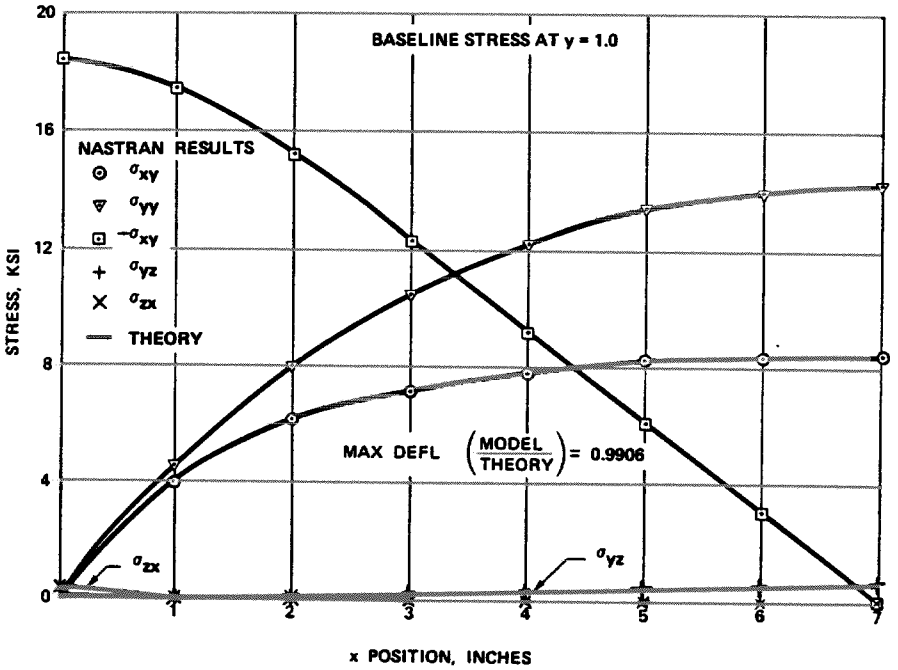

Figure 31 - Plate Bending Model, All 20-Node HEXA Elements

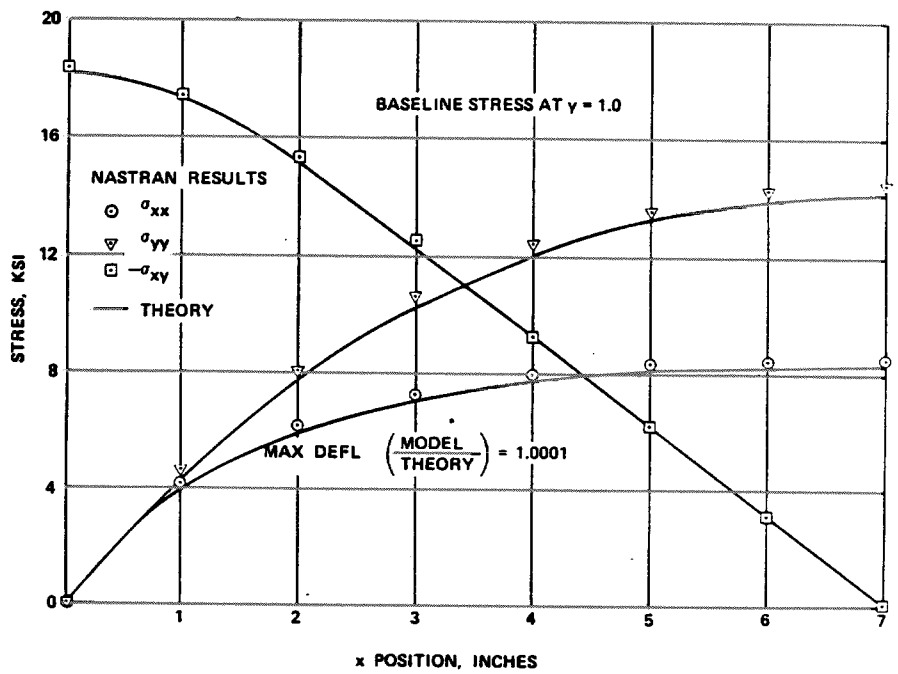

Figure 32 - Plate Bending Model, All QUAD8 Elements

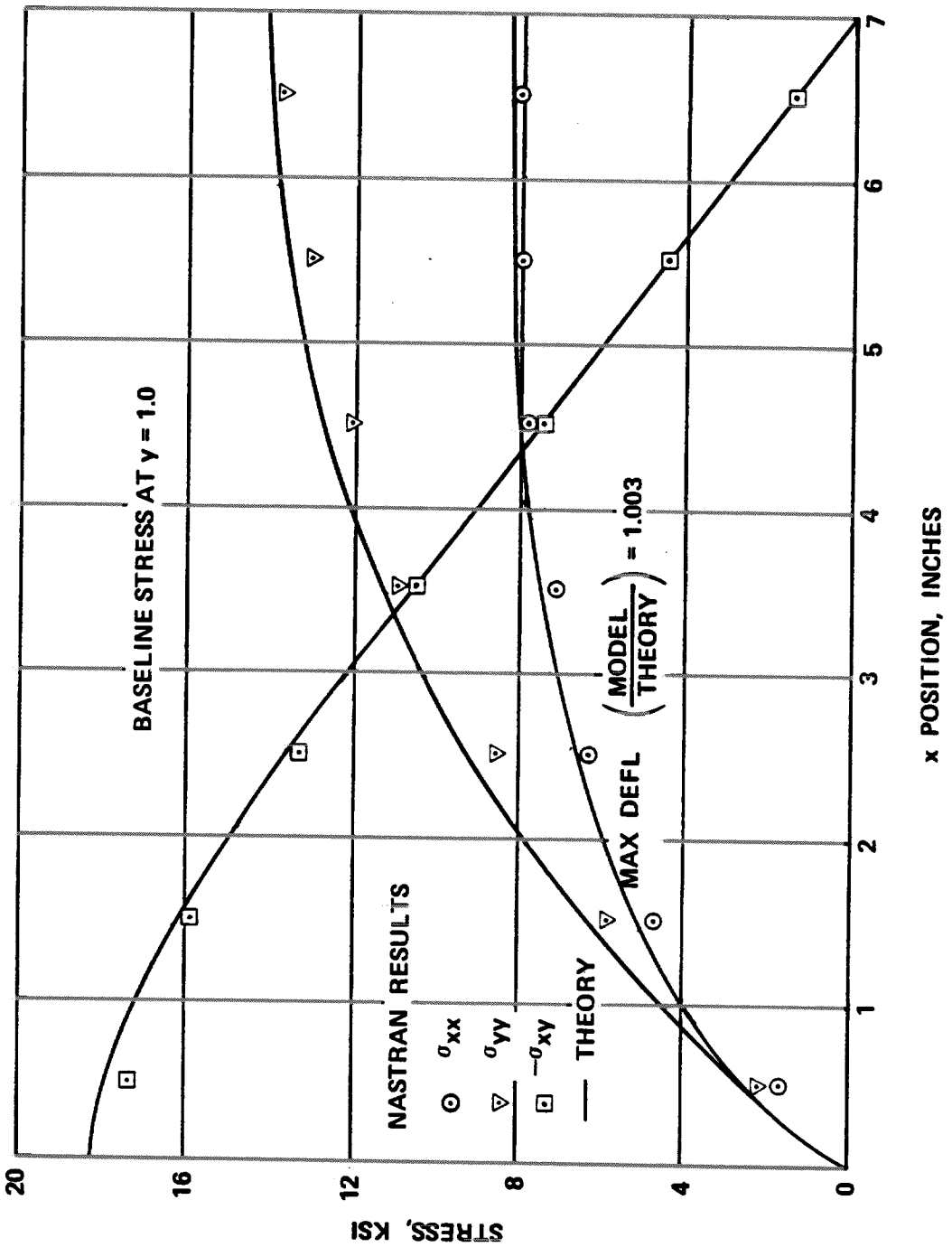

Figure 33 - Plate Bending Model, All QUAD4 Elements

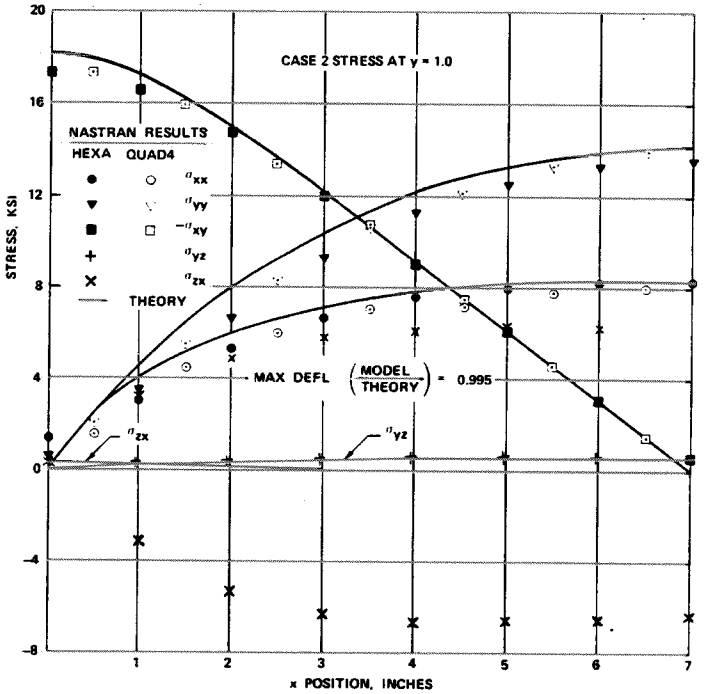

Figure 34 - Plate Bending Model, HEXA and QUAD4 Elements (Case 2 Stress at y = 1)

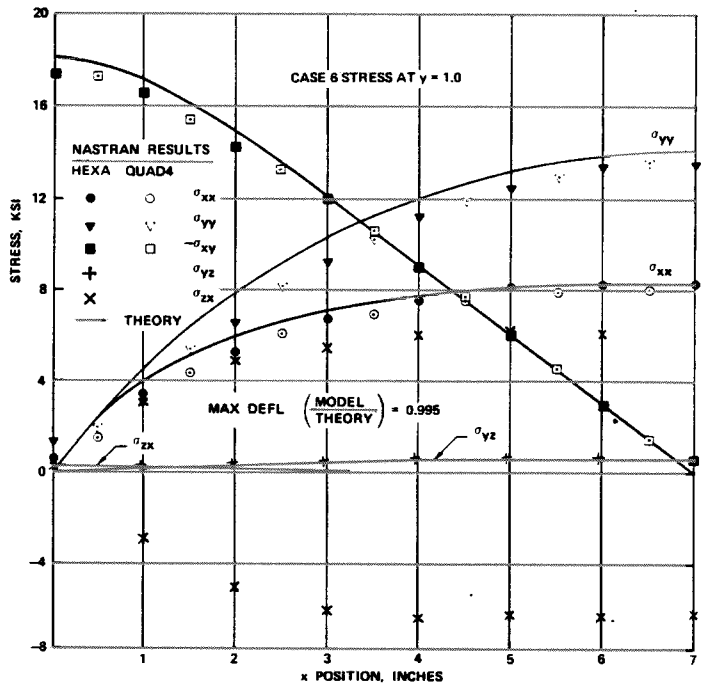

Figure 35 - Plate Bending Model, HEXA and QUAD4 Elements (Case 6 Stress at y = 1)

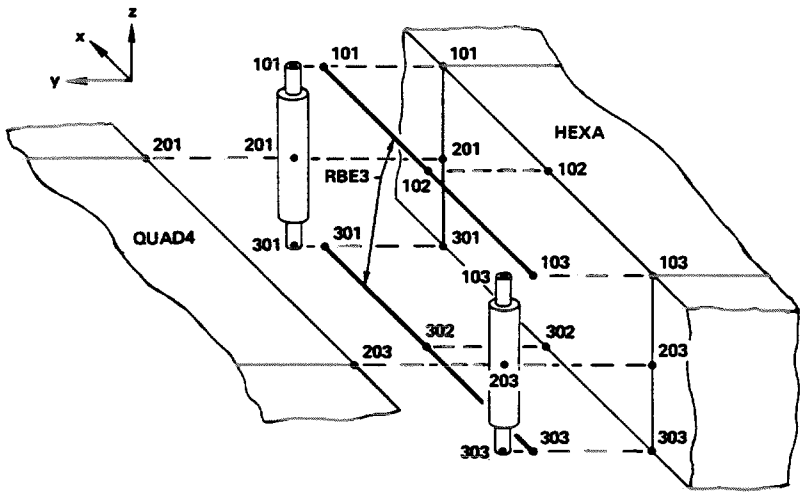

RBAR	EID	GA	GB	CNA	CNB	CMA	CMB		
RBAR	1	201	101	123456			12		
RBAR	2	201	301	123456			12		
RBAR	3	203	103	123456			12		
RBAR	4	203	303	123456			12		

RBE3	EID		REFGRID	REFC	WT1	C1	G1,1	G2,1	
RBE3	5		102	2	1.	1234	101	103	
RBE3	6		302	2	1.	1234	301	303	

Figure 36 - Case 12 Typical Interface, H20Q4 Model

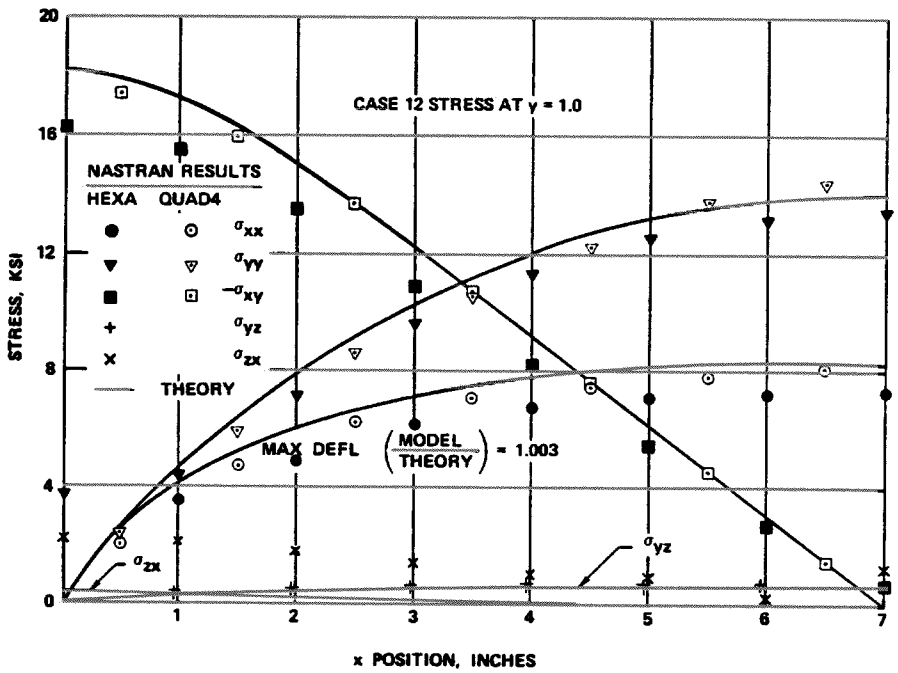

Figure 37 - Plate Bending Model, HEXA and QUAD4 Elements (Case 12 Stress at y = 1)

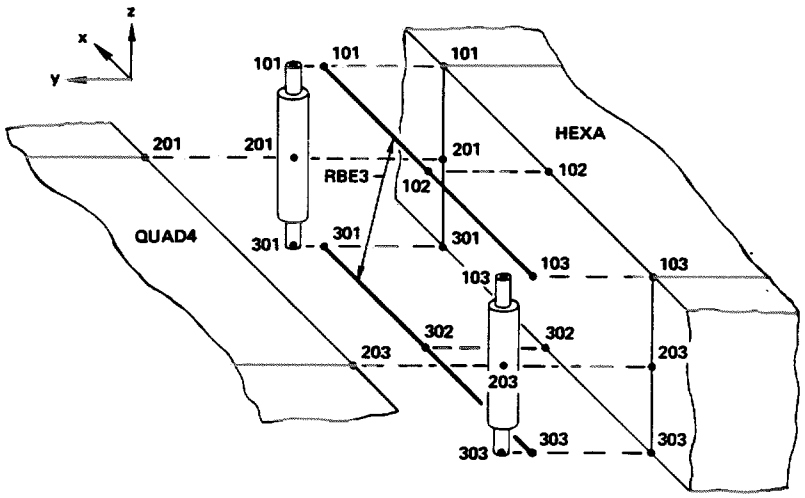

RBAR	EID	GA	GB	CNA	CNB	CMA	CMB		
RBAR	1	201	101	123456			12		
RBAR	2	201	301	123456			12		
RBAR	3	203	103	123456			12		
RBAR	4	203	303	123456			12		

RBE3	EID		REFGRID	REFC	WT1	C1	G1,1	G2,1	
RBE3	5		102	12	1.	1234	101	103	
RBE3	6		302	12	1.	1234	301	303	

Figure 38 - Case 13 Typical Interface, H20Q4 Model

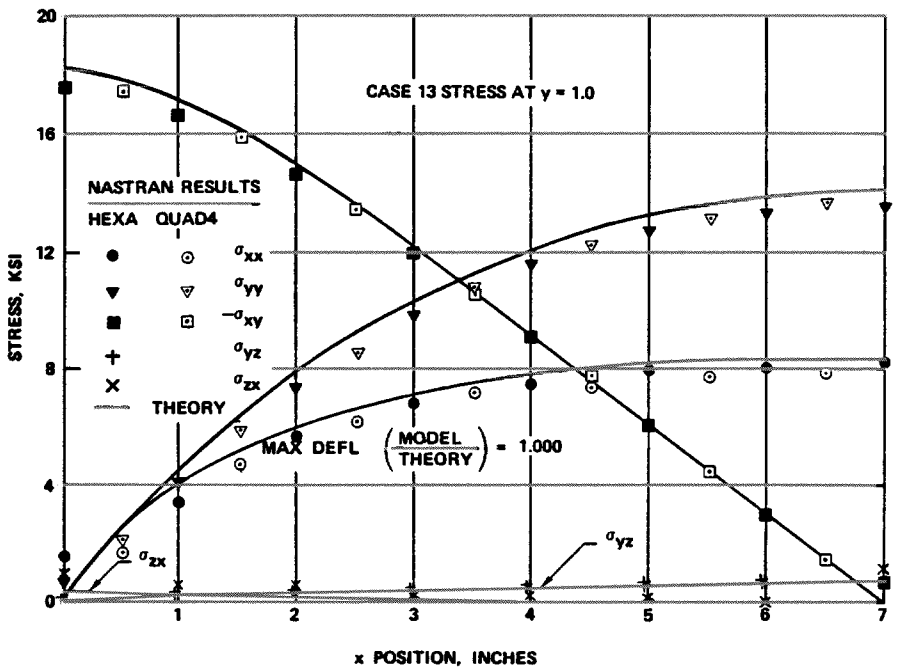

Figure 39 - Plate Bending Model, HEXA and QUAD4 Elements (Case 13 Stress at y = 1)

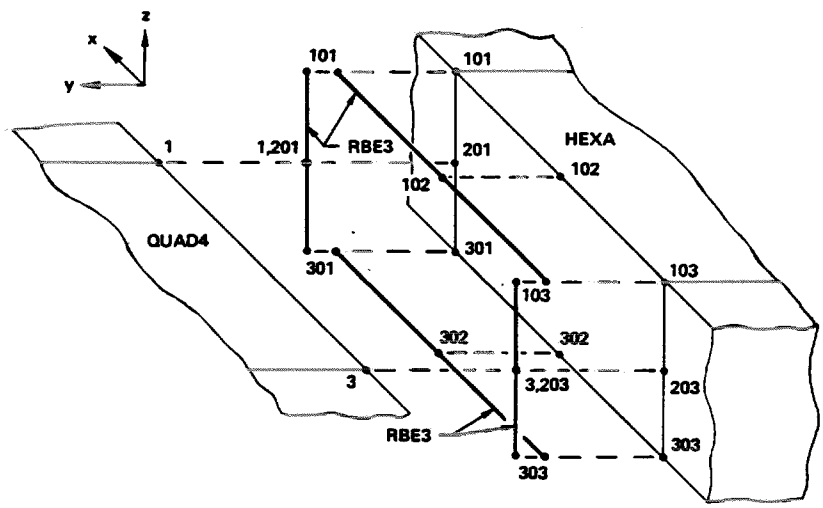

RBE3	EID		REFGRID	REFC	WT1	C1	G1,1	G2,1	
RBE3	1		1	12345	1.	1236	101	201	+RB1
+RB1	301								
RBE3	2		3	12345	1.	1236	103	203	+RB2
+RB2	303								
RBE3	3		102	12	1.	1234	101	103	
RBE3	4		302	12	1.	1234	301	303	

Figure 40 - Case 14 Typical Interface, H20Q4 Model

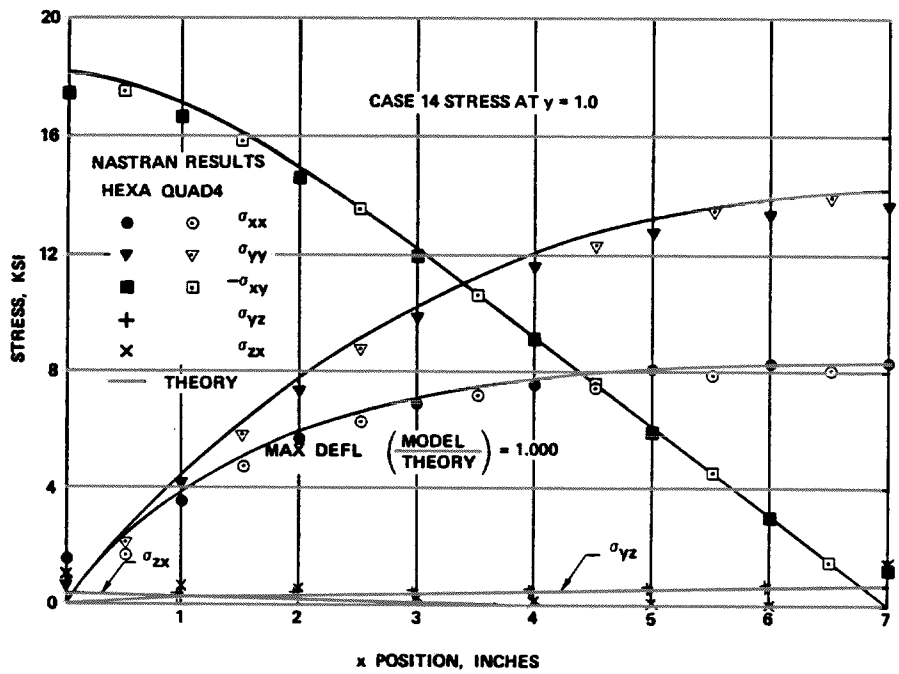

Figure 41 - Plate Bending Model, HEXA and QUAD4 Elements
(Case 14 Stress at y = 1)

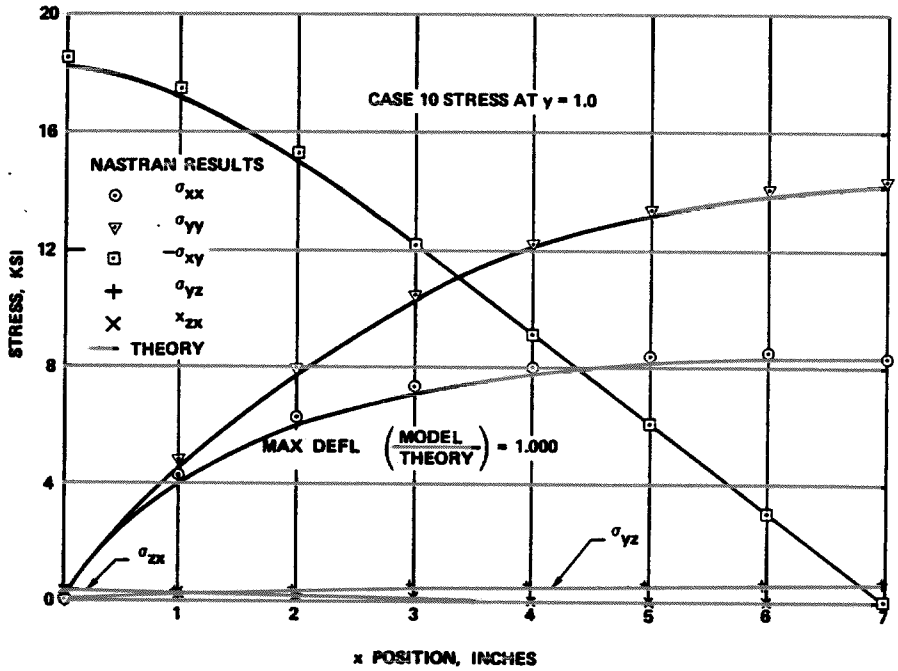

Figure 42 - Plate Bending Model, HEXA and QUAD8 Elements
(Case 10 Stress at y = 1)

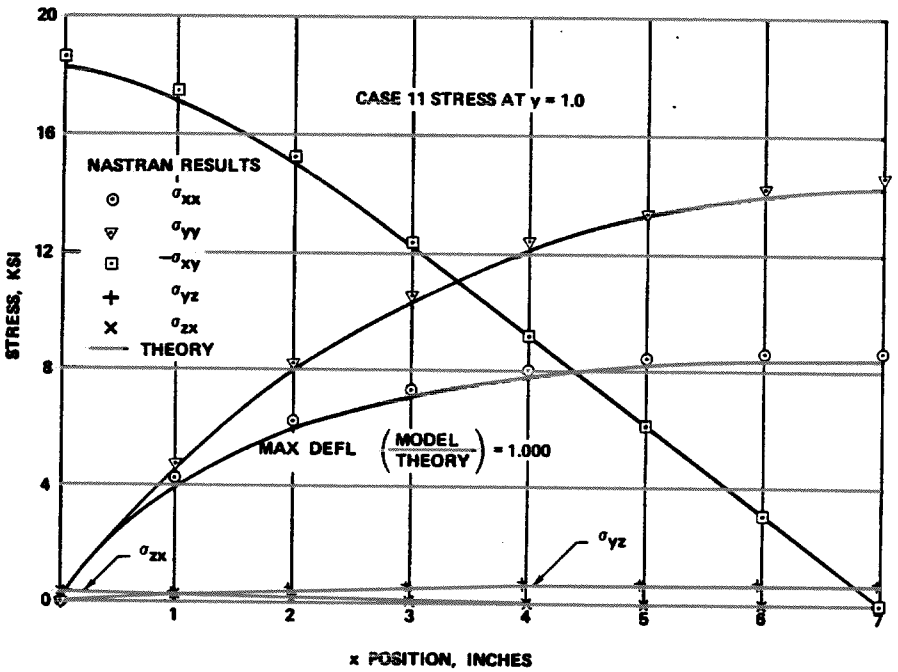

Figure 43 - Plate Bending Model, HEXA and QUAD8 Elements
(Case 11 Stress at y = 1)